1983-09

Numerical simulation of the forcing of monsoon surges by mid-latitude baroclinic waves

Baker, Beverley J.

Monterey, California. Naval Postgraduate School

NAVAL POSTGRADUATE SCHOOL
Monterey, California

THESIS

NUMERICAL SIMULATION OF THE FORCING OF
MONSOON SURGES BY MID-LATITUDE BAROCLINIC WAVES

by

Beverley J. Baker

September 1983

Thesis Advisor: R. T. Williams

Approved for public release; distribution unlimited

REPORT DOCUMENTATION PAGE		READ INSTRUCTIONS BEFORE COMPLETING FORM
1. REPORT NUMBER	2. GOVT ACCESSION NO.	3. RECIPIENT'S CATALOG NUMBER
4. TITLE (and Subtitle) Numerical Simulation of the Forcing of Monsoon Surges by Mid-Latitude Baroclinic Waves		5. TYPE OF REPORT & PERIOD COVERED Master's Thesis September 1983
		6. PERFORMING ORG. REPORT NUMBER
7. AUTHOR(s) Beverley J. Baker		8. CONTRACT OR GRANT NUMBER(s)
9. PERFORMING ORGANIZATION NAME AND ADDRESS Naval Postgraduate School Monterey, California 93943		10. PROGRAM ELEMENT, PROJECT, TASK AREA & WORK UNIT NUMBERS
11. CONTROLLING OFFICE NAME AND ADDRESS Naval Postgraduate School Monterey, California 93943		12. REPORT DATE September 1983
		13. NUMBER OF PAGES 109
14. MONITORING AGENCY NAME & ADDRESS(If different from Controlling Office)		15. SECURITY CLASS. (of this report)
		15a. DECLASSIFICATION/DOWNGRADING SCHEDULE

16. DISTRIBUTION STATEMENT (of this Report)

Approved for public release, distribution unlimited

17. DISTRIBUTION STATEMENT (of the abstract entered in Block 20, if different from Report)

18. SUPPLEMENTARY NOTES

19. KEY WORDS (Continue on reverse side if necessary and identify by block number)

Numerical Weather Prediction
Winter Monsoon
Monsoon Surge
Topographic Effects
Baroclinic Instability

20. ABSTRACT (Continue on reverse side if necessary and identify by block number)

A global, six-level, primitive equation model was numerically integrated to examine the interaction of a mid-latitude baroclinic wave with several different mountain-valley configurations. The purpose was to determine the contribution of a well-developed baroclinic wave to the initiation of a monsoon surge. It was found that these waves can initiate a surge. Such surges are weak and limited in extent but they

20. <u>Abstract</u> (Continued)

do exhibit the characteristics of observed monsoon surges. The
latitudinal location of the east-west mountain range has a large impact
on the strength of the disturbance and thus on the initiation of the
surge. However, the size of the valley is not an important consideration.
The surge is strongest at the lowest levels and dissipates rapidly with
height. Overall results indicate surge forcing by the baroclinic wave
is possible but other forcing mechanisms are necessary in order to
simulate the stronger, more extensive surges observed during the
winter monsoon.

Numerical Simulation of the Forcing of
Monsoon Surges by Mid-Latitude Baroclinic Waves

by

Beverley J. Baker
Captain, United States Air Force
B.S., University of Washington, 1974

Submitted in partial fulfillment of the
requirements for the degree of

MASTER OF SCIENCE IN METEOROLOGY

from the

NAVAL POSTGRADUATE SCHOOL
September 1983

ABSTRACT

A global, six-level, primitive equation model was numer-
ically integrated to examine the interaction of a mid-lati-
tude baroclinic wave with several different mountain-valley
configurations. The purpose was to determine the contribu-
tion of a well-developed baroclinic wave to the initiation
of a monsoon surge. It was found that these waves can ini-
tiate a surge. Such surges are weak and limited in extent
but they do exhibit the characteristics of observed monsoon
surges. The latitudinal location of the east-west mountain
range has a large impact on the strength of the disturbance
and thus on the initiation of the surge. However, the size
of the valley is not an important consideration. The surge
is strongest at the lowest levels and dissipates rapidly
with height. Overall results indicate surge forcing by the
baroclinic wave is possible but other forcing mechanisms are
necessary in order to simulate the stronger, more extensive
surges observed during the winter monsoon.

TABLE OF CONTENTS

5

LIST OF FIGURES

ACKNOWLEDGEMENT

I. INTRODUCTION

In recent years meteorologists have given considerable attention to the Asian winter monsoon. Described by Chang and Lau (1980) as "one of the most energetic heat engines in driving the earth's atmosphere", the winter monsoon is the most distinctive component of the Northern Hemisphere winter circulation. Its fundamental, large scale structure has long been observed, however, much about the monsoon remains unknown. The role of the monsoon in the interaction of the mid-latitude and tropical regions, the variability of the monsoon and the forcing of small scale monsoonal variations are all areas of active research.

A monsoon may be defined as a three dimensional, plane-tary scale wind regime that reverses direction seasonally. In the case of the monsoon, the establishment of the summer cyclone and winter anticyclone is governed by land-sea dif-ferences and the varying position of the sun. Essentially, it is the seasonal replacement of one persistant circulation system by an equally persistant but opposite system. The development of these circulations closely links the monsoon, particularily that of east Asia, to regional topography.

The long, clear nights of the Siberian winter allow strong radiational cooling and the subsequent formation of a shallow, cold layer of surface air. Persistent cold air advection throughout the troposphere further contributes to the formation of a surface high. The winter monsoon, which dominates the entire Asian continent, is characterized by this intense, cold polar anticyclone. The resulting north-northeasterly surface flow extends over all of eastern Asia and southward across the equator. The Himalayan Mountains restrict the southward movement of the cold lower tropos-pheric air and provide an effective barrier to the mixing of the cold continental airmass with the warm tropical airmass of southern Asia. As the anticyclone becomes established over Siberia, a surface cyclone develops over the "maritime continent" region of Indonesia and Malaysia as a major plan-etary scale convective area is shifted eastward from its summer position near India (Ramage, 1971).

An analysis of the monthly mean velocity potential field at 200 mb for December 1974 by Chang and Lau (1980) shows a broad region of divergence over the maritime continent. This is indicative of deep rising motions and large scale overturning of the atmosphere. Their analysis also shows a

11

region of maximum convergence over northern China in the
vicinity of the Siberian anticyclone. (Note that for large
scale flow the divergence pattern is approximately given by
the velocity potential.) Upper-level convergence is also
evident in the equatorial west Pacific Ocean and over the
east African coast. Although much weaker, these latter two
areas indicate the existence of a Walker circulation.
Ascending over the maritime continent, one branch flows
westward across the Indian Ocean and Arabian Sea, while
another branch flows eastward to descend over the western
Pacific Ocean.

Thus the winter tropospheric circulation in this region
is dominated by a strong local Hadley cell; a thermally
direct circulation involving descent in the cold air over
the northern anticyclone, southward surface flow, ascent of
warm air over the maritime continent and northward return
flow at 200 mb.

The large-scale components of the monsoon are consistent
and identifiable from year to year, but they are not static.
The primary features not only vary in strength and location
on an annual time scale but there are small time scale vari-
ations in the velocity, temperature and pressure fields as

12

well. One particular event that can be linked to short time scale variations is the monsoon surge. Also known as "cold surges" these events occur at intervals of several days to two weeks during the winter monsoon (Lim and Chang, 1981).

The characteristics and effects of the monsoon surge have been discussed in several observational studies at both the synoptic and planetary scales by Danielson and Ho (1969), Chang et al (1979), Murakami (1979), Chang and Lau (1980,1982) and Chang et al (1983). The following sequence of events for a monsoon surge is taken from these studies.

Prior to the occurrence of a monsoon surge there is intense, deep cold air advection over northern Asia accompanied by the passage of a mid-tropospheric trough that intensifies rapidly over northern Japan. The resulting increase in baroclinicity is associated with anticyclogenesis over Siberia and cyclogenesis in the strong baroclinic zone off the east China coast. The east Asian Hadley circulation is strengthened through increased subsidence as the anticyclone intensifies. The east Asian subtropical jet accelerates near Japan as the intensification of the Hadley circulation increases upper-level ageostrophic flow. The west Asian jet streak varies inversely with the east Asian jet and so decreases in strength over Afghanistan and Pakistan.

The monsoon surge is initiated as the upper-level trough moves eastward and the pressure gradient across the east China coast tightens. The normal geostrophic balance of the anticyclonic flow is broken since the pressure gradient force is now greater than the Coriolis force and a rapid cross-isobaric flow from high to low pressure begins. This accelerating flow towards lower pressures at lower tropospheric levels is the monsoon surge. Following the surge, an increase in the northeasterly flow can be traced to the equatorial regions within 12-24 h. Within one to two days convection in the equatorial region intensifies and sustains the already enhanced Hadley circulation. The upper-level outflow from the equatorial South China Sea accelerates not only northward, but within one day of the surge accelerates east and west along the equator, thus strengthening the Walker circulation. The surge ends as the mid-latitude trough/ridge pattern moves sufficiently eastward so that subsidence no longer occurs over the anticyclone.

Lim and Chang (1981) and Chang, Chen and Millard (1983) suggest that the monsoon surge is characterized by two stages separated by an interval of a few hours to one day, depending on the location of the observing station. The

first stage is the pressure surge, or leading edge of the downward accelerating air, with a propagation speed characteristic of gravity waves. The second stage, which moves at advective time scales, is due to a frontal passage and is characterized by a sharp decrease in the surface dewpoint.

Few studies have been done to determine the cause or nature of the forcing that precipitates a monsoon surge. Lim and Chang (1981) used the linearized shallow-water equations on an equatorial beta-plane in an analytical study of monsoon response to a transient mass source that simulated intense anticyclogenesis. Their results showed that such mid-latitude forcing excites mainly Rossby waves after an initial period of gravity wave type motions associated with strong northerly winds. They suggested that pressure forcing, using equatorial beta-plane dynamics, can explain the large features of synoptic scale motions in the eastern monsoon region. However, they do not consider other effects such as orography or a variable mean zonal wind. Nor does their method account for the shallow vertical structure of monsoon surges or upper tropospheric response to the surge.

The purpose of this study is to examine the interaction of topography, specifically a high east-west mountain range,

with a mid-latitude baroclinic wave. The purpose will be to determine the contribution of the baroclinic wave to the initiation of monsoon surges. A global, six-level primitive equation model will be used to simulate the meteorological conditions prior and subsequent to surge initiation. Initial conditions will include a strong baroclinic jet north of the mountain range and a small disturbance in the mean current; the disturbance will grow through baroclinic instability. Several mountain-valley configurations will be used to study the surge and numerical solutions will be compared with observed monsoonal surges.

II. DESCRIPTION OF MODEL

The numerical model used in these experiments is a ver-
sion of the UCLA potential enstrophy conserving, general
circulation model for an adiabatic, dry and frictionless
atmosphere. The governing equations for this model are the
primitive equations: the horizontal momentum equation,
thermodynamic energy equation, surface pressure tendency
(continuity) equation, and the hydrostatic equation. These
are given in Appendix A. The design and dynamic processes
of the model are fully discussed by Arakawa and Lamb (1977,
1981). A summary of the version used for this experiment is
presented here.

A. THE HORIZONTAL GRID

The prognostic variables, wind(U,V), temperature (T),
and terrain pressure(Π), are staggered horizontally accord-
ing to Arakawa's Scheme 'C' (Fig. 1). This grid arrange-
ment, although using more computer time than an unstaggered
grid, gives a better structure for the shorter waves that
arise due to geostrophic adjustment, nonlinear interaction
or mountain effects. Resolution is 2.5° long by 4.0° lat

17

using a 36 x 46 spherical grid. The computational domain is a 90° sector of the globe with cyclic continuity imposed at the east and west boundaries.

In spherical coordinates the poles are singular points. Since velocity components cannot be defined at the poles, they are taken as Π-points. Due to the convergence of the meridians towards the poles a very short time step would normally be required to insure computational stability.   To allow a longer time step, longitudinal averaging is done for selected terms in the equations that govern gravity wave propagation.   To do this the zonal pressure gradient and zonal mass flux are expanded into a Fourier series around each latitude circle, then the amplitude of each wave compo-nent is reduced by the factor S. This technique smooths the gradients of the meteorological fields rather than their Fourier expansions.   The smoothing operator S is applied only at higher latitudes (where S<1) and is given by:

$$S = \frac{\Delta\lambda}{\Delta\phi} \frac{\cos\phi}{\sin(n\Delta\lambda/2)}$$

(Symbol definitions are given in Appendix 3)

18

B. THE VERTICAL GRID

The equations used in this model are written using the vertical sigma coordinate:

$$\sigma = \frac{P - P_t}{\Pi} \qquad \text{where} \quad \Pi \equiv P_s - P_t$$

P_s is the surface pressure and P_t is the pressure at the tropopause.

The vertical domain extends from the earth's surface to 200 mb. Variables are staggered vertically (Fig. 2) in six layers equally spaced in sigma. The lower boundary, $\sigma = 1$, follows topography, where the surface pressure is defined. At both the upper and lower boundaries vertical velocity, $\dot{\sigma}$, vanishes. The prognostic variables $(u, v, \Gamma,)$ are computed at mid-layer, while geopotential, $\bar{\phi}$, vertical velocity, $\dot{\sigma}$, and terrain pressure, Π are computed diagnostically on sigma levels.

C. FINITE DIFFERENCING SCHEMES

The time differencing methods used in this model are the fourth-order space differencing scheme and the Matsuno scheme (also called the Euler-backward scheme). One Matsuno

19

time step is performed followed by four centered time steps. The Matsuno scheme is used to eliminate the computational mode of the centered scheme and because it selectively damps high frequency waves. The time step used here is 360 s.
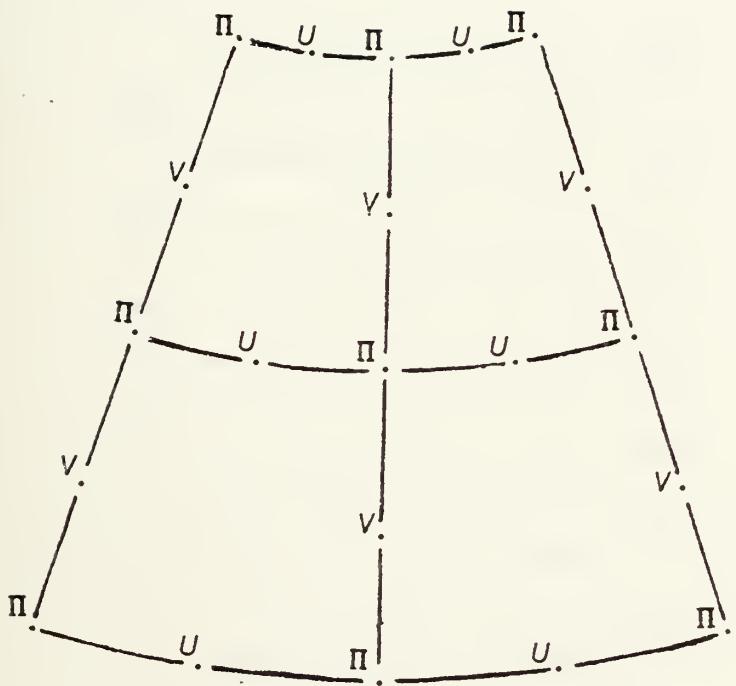
Figure 1.   Horizontal Distribution of Variables on a
            Spherical Grid.
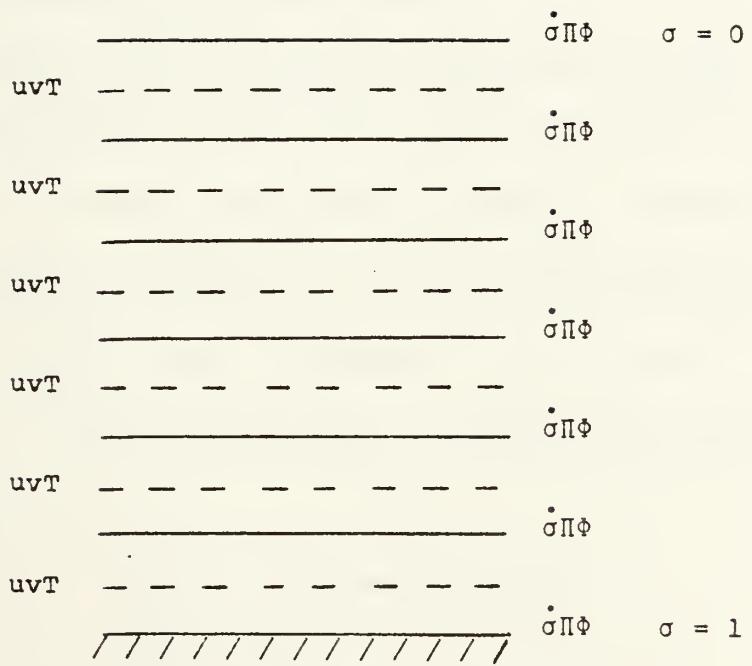
Figure 2. Distribution of Prognostic Variables in the Vertical. Solid lines are σ-levels, dashed lines are at mid-layer.

III. MODEL INITIALIZATION

The model uses an analytical initialization scheme developed by Major J. L. Hayes,[1] USAF. A small perturbation is superimposed on a horizontally and vertically varying mean current, then allowed to grow through baroclinic instability. The scheme was derived specifically for flow over a flat earth; initialization over high terrain requires an adjustment to the scheme and is discussed separately.

A. INITIALIZATION OF THE MEAN FLOW

A baroclinic Bickley jet is situated at 45°N, where it reaches a maximum velocity of 46 m/s at 200 mb. The initial mean surface flow has the same latitudinal variation as the jet; it reaches a maximum of 5 m/s at 45°N and decreases to zero at the poles. The v-component of the wind is initially set to zero. The surface wind is described by the Bickley jet profile:

$$\overline{U}_s(\phi) = \overline{U}_m \operatorname{sech}^2(\gamma(\phi-\phi_0))$$

$$\overline{V}_s(\phi) = 0$$

---

[1] Personal communication, present affilitation Detachment 1, HQ AWS.

The upper-level wind has the same latitudinal profile:

$$\overline{U}_u(\phi, P(\sigma, \phi)) = \overline{U}_m \ \text{sech}^2(\gamma(\phi-\phi_0)) \left(\frac{\ln(P_s/P)}{\ln(P_s/P_m)}\right)$$

$$\overline{V}_u(\phi, P(\sigma, \phi)) = 0$$

The last term on the right produces the vertical shear. The initial wind at any latitude and level is calculated by adding the upper-level and surface winds.

Since the mean flow is in geostrophic balance, the surface pressure is calculated by integrating the geostrophic wind equation:

$$\overline{P}_s(\phi) = \overline{P}_s(\phi_0) \left[\exp\left(-\frac{af_0\overline{U}_s}{RT_0\gamma} \tanh(\gamma(\phi-\phi_0))\right)\right]$$

The value of T_0, 288K, is taken from the NACA standard atmosphere using a standard surface pressure of 1013.25 mb.

Temperature, except at the surface, is determined by integrating the geostrophic thermal wind equation:

$$\overline{T}(p,\phi) = \overline{T}(p,\phi_0) - \frac{\overline{U}_m \ a \ 2\Omega}{R \ \ln(P/P_m)} \int_{\phi_0}^{\phi} \sin\phi \ \text{sech}^2(\phi-\phi_0) \ d\phi$$

Integrals are computed using the Simpson Rule approximation.

The vertically varying term $T(p,\phi)$ is obtained from the NACA standard atmosphere:

$$\overline{T}(p,\phi_0) = \overline{T}(p_0,\phi_0) - \Gamma z$$

$$\text{where:} \quad z = \frac{T_0}{\Gamma}\left(1 - \left(\frac{p}{p_0}\right)^{\Gamma R/g}\right)$$

The constants are defined in Appendix B.

B.   INITIALIZATION OVER HIGH TERRAIN

The mountains in this model are intended to be a very simple representation of the Himalayan Range. The mountains extend east to west across the grid section with a maximum elevation of 3000 m. The longitudinal span is 16° or approximately 1600 km.

The mountains were initialized at full height without any growth period. The equations used to produce the mountains are relatively simple and produce a knife-edged range:

$$\Phi = C_1(\phi)\Phi_f = \begin{cases} .25 \ \Phi_f & \text{at } |\phi-\phi_1| = 2\Delta\phi \\ .75 \ \Phi_f & \text{at } |\phi-\phi_1| = 2\Delta\phi \\ \Phi_f & \text{at } \phi = \phi_1 \end{cases}$$

The immediate initialization of the terrain does lengthen the geostrophic adjustment time. However, the model is run

for 72 h prior to creating the valley and it is reasonable to assume the longer adjustment period will have no serious effect on the attempted simulation of the monsoon surge. Using the mean flow initialization scheme without a mountain growth period resulted in a large scale, north-south oscillation in the pressure field. There was little evidence of damping during a 96-h model run. To solve this problem the surface pressures at mountain grid points were adjusted for height above mean sea-level. Using the hydrostatic equation and the adiabatic lapse rate for the NACA standard atmosphere, the following equation was developed for a new (mountain) surface pressure in terms of the old (flat earth) surface pressure:

$$\overline{P}_s(\text{new}) = \overline{P}_s(\text{old}) \left(1 - \frac{\Gamma z}{T_0} \right)^{g/RT}$$

The new surface pressure is used to re-calculate wind and temperature values at each mountain grid point. No oscillation was evident when the adjusted values were used in the initialization.

As the monsoon surge is expected to occur almost immediately following the creation of the valley, the geostrophic

26

adjustment time cannot be neglected at this point. There-
fore, the valley is "built" over a 12-h period to minimize
the time required for geostrophic adjustment. The method
used is based on the scheme developed by Hayes (previously
cited) for raising terrain height during a model run. To
build the valley however, the method is reversed:

$$\Phi = C_1(\phi)\Phi_f\left[1 - C_2(\tau)G(\lambda)\right]$$

The function $C_2(\tau)$ is defined:

$$C_2(\tau) = \begin{cases} \sin^2\left(\dfrac{\pi}{2}\dfrac{\tau-\tau_i}{\tau_f-\tau_i}\right) & \tau_i < \tau \leq \tau_f \\\\ 1 & \tau \leq \tau_i \text{ and } \tau > \tau_f \end{cases}$$

The function $G(\lambda)$ is defined:

$$G(\lambda) = \begin{cases} 1 & \lambda_1 < \lambda < \lambda_2 \\\\ \dfrac{\lambda-\lambda_1-2\Delta\lambda}{-2\Delta\lambda} & (\lambda-2\Delta\lambda) \leq \lambda \leq \lambda_1 \\\\ \dfrac{\lambda_2+2\Delta\lambda-\lambda}{2\Delta\lambda} & \lambda_2 \leq \lambda \leq (\lambda_2+2\Delta\lambda) \\\\ 0 & \text{elsewhere} \end{cases}$$

λ_1 and λ_2 are the west and east edges of the valley respec-
tively. Where no valley is built, $G(\lambda) \equiv 1$. The valley
walls are sloped over two grid-lengths $(2\Delta X)$, and the valley
floor is at mean sea-level (0 m).

C. THE PERTURBATION

The perturbation is a standard barotropic disturbance. It consists of a weak longitudinal sine wave with maximum latitudinal amplitude at 45°N. The vertical amplitude is one-tenth the earth's radius. The perturbation is described by:

$$\Phi' = f_0 \left(A \sin(n\lambda) \sin^2(2\phi) \right)$$

The following perturbation quantities are derived using the hydrostatic equation and geostrophic wind equation:

$$P' = -\frac{\overline{P}\Phi'}{RT} = -\frac{Pf_0}{RT}\left(A \sin(n\lambda) \sin^2(2\phi) \right)$$

$$U' = -\frac{1}{af_0}\frac{\delta\Phi'}{\delta\phi} = -\frac{1}{a}\left(A \sin(n\lambda) \, 2\sin(4\phi) \right)$$

$$V' = \frac{1}{af_0 \cos}\frac{\delta\Phi'}{\delta\phi} = \frac{1}{a\cos\phi}\left(nA \cos(n\lambda) \sin^2(2\phi) \right)$$

$$T' \equiv 0$$

The total fields are calculated by adding the perturbation quantities to the mean current. The total fields will then be integrated in time to arrive at the required forecast values.

IV.   ANALYSIS OF RESULTS

A.   EXPERIMENTS 1 & 2:   CONTROL RUNS

Two control runs were made for comparison with subsequent model runs. The first run uses a flat earth while the second includes a 3000-m east-west mountain range centered at 30°N.   Both runs are initialized with the baroclinically unstable mean flow and the barotropic disturbance discussed in Chapter 3.   Model times given   are based on the time (h) at which the disturbance is introduced into the mean flow.

The first run follows the development of the disturbance independent of terrain effects.   Sea-level pressure fields for 60, 72, 84 and 96 h are shown schematically in Figs. 3 and 4.   Potential temperature fields for the same times are shown in Figs. 5 and 6.   Since a pie-shaped section of the globe is represented in cartesian coordinates there is some distortion of the fields.   This is primarily evident in the tight north-south pressure gradients which, for comparable wind velocities, appear weaker in the east-west direction.

The disturbance is strictly limited to the mid-latitudes with a very flat pressure gradient in both the polar and the

29

tropical regions. The disturbance moves eastward at a con-
stant velocity of approximately 8.5° every twelve hours.
Wave development is realistic with a 995 mb low and a 1023
mb high developing after 78 h.

Development of the disturbance in the wind and tempera-
ture fields closely parallels that of the pressure field,
although the temperature and potential temperature data dis-
play far more short wave noise. As no surface frictional
dissipation, diffusion, or smoothing techniques are used in
the model, some noise in the results is expected. The large
scale temperature features remain discernable throughout the
six day (144 h) run but the the small scale features are
masked by noise after 126 h, especially at higher levels.
(Temperature and wind velocities are plotted on sigma sur-
faces; 'higher levels' refers to increased height, or lower
sigma values.)

After 96 h particularily strong cyclogenesis begins to
occur. At 114 h the cyclones intensify rapidly and the
ridge is drastically weakened. While diffusion or smoothing
applied to the fields would decrease the strong gradients
caused by cyclogenesis, they would also weaken the gradients
of pressure and temperature which could contribute to possi-

ble monsoon surges. For this reason neither method is used. A linear drag term was applied to the winds in the lowest level, however it had no discernable effect on the strong cyclogenesis.

The mountain range used in second control run is the basis for all subsequent terrain configurations. Fig. 7 gives a three-dimensional representation of the range. (Note the vertical scale is greatly exaggerated.) The data from this run are used to determine the time and location at which the valley is to be created. The requirements are: (1) a high pressure center to the northeast (to be consistent with the Siberian anticyclone) and (2) a sea-level pressure difference of 25 mb between the high and low pressure centers. The latter requirement ensures an adequate northwesterly current to initiate a monsoonal surge.

Sea-level pressure and potential temperature fields for 60, 72, 84 and 96 h are shown in Figs. 8 through 11. Eastward movement of the disturbance is again 8.5° per twelve hours. The most noticeable difference between this experiment and the first is a series of weak highs and lows that have developed along the northern slope of the mountains. These disturbances migrate eastward at a speed comparable to the mid-latitude wave.

Development of the wave is slower than in the previous case. At 78 h a 999 mb low and a 1019 mb high have developed, giving a pressure difference of 20 mb compared to 28 mb earlier. This represents an overall weakening of the disturbance and is not due to the weakening of either the high or low centers individually. It appears the mountain range may have a stabilizing effect on the growing disturbance. The required 25 mb pressure difference is reached at 84 h. Since a twelve hour period is required to create the valley, growth will be initiated at 72 h model time in subsequent runs. Since the valley must be located east of the anticyclone in order to take advantage of the associated northwest flow, the western edge of the valley is placed directly south of the leading portion of northwesterly winds at 84 h.

Development of the disturbance in the potential temperature and wind fields is very similar to the first run. There is a maximum in potential temperature over the mountains but this is simply due to the increased elevation.

The small scale noise apparent in the potential temperature fields of the first run also appear in this experiment although at a later time, possibly due to the much slower

32

development of the cyclone-anticyclone system. The strong cyclogenesis and intense pressure gradients also appear later in the second model run. Wave development is approximately six hours slower when the mountains are included and this corresponds to the time lag observed in the cyclogenesis and noise growth.

It should be noted that potential temperature is used in the analysis of model results since its fields will not include effects of the adiabatic processes occurring in flow over mountains.

B. EXPERIMENT 3

The initialization for this experiment, and all subsequent experiments, is provided by the same analytic scheme used in the control runs. Terrain consists of an east-west mountain range centered at 30°N. The valley, built between 72 and 84 h, is twelve gridlengths wide or nearly one-third the length of the mountain range (Fig. 12). The critical time period for the occurrence of a surge will be the first 24 h after the valley is completed (84-108 h). It is during this period that the anticyclone is located northwest of the valley.

33

Development of the disturbance through 72 h is described by control run #2. The sea-level pressure field at 84 h shows a trough extending across the valley and along the northern slope of the eastern range. At the same time a small, high pressure ridge can be seen in the northwest region of the valley. For the next twelve hours the ridge continues to build southward until, at 96 h, it extends the length of the western valley wall splitting the trough into two separate low centers. The pressure gradient in the tropical region south of the valley has also increased (Fig. 13). As the ridge continues to expand southward, the eastern portion of the trough develops a very strong, tight pressure gradient in the valley and along the northern mountain slopes (Fig. 14). The ridge continues to strengthen and remains located along the western wall through 114 h. After this time the anticyclone moves eastward to a position due north of the valley and the ridge begins to weaken.

Also noted in the results is an oscillation in the intensity of the pressure field. It begins when valley growth is initiated and has a period of approximately 24 h. The observed oscillation is possibly the result of gravity waves set up by the relatively sudden (12 h) creation of the valley.

34

The second stage of the monsoon surge was earlier described as being characterized by a sharp drop in surface dewpoint. Since this is a dry model, and as observational studies (Chang et al, 1979, Chu, 1978) show this stage can also be associated with a drop in surface temperatures, the potential temperature fields are analyzed for possible surge characteristics. (Beyond this point 'temperature' refers to potential temperature unless otherwise stated.)

In agreement with the development of the surface pressure ridge, a weak tongue of cold air has formed along the western valley wall at 84 h. However, no similar gradient exists along the eastern wall (Fig. 15).

Twelve hours after the valley is completed, the cold air has reached the southern valley boundary. Minimum temperature at 24°N has dropped from 310K at 84 h to 303K at 96 h. A tight temperature gradient exists along the western side of the cold air intrusion and also along the northern mountain slopes where temperatures have remained relatively constant. The cold air tongue can easily by seen at the two lowest levels (Fig. 16). At the mid-levels a very slight tightening of the gradient can be seen over the western valley wall when compared to the eastern wall, but only over

35

the northern half of the valley. At the highest two levels, gradients over the two valley walls are nearly identical so that the apparent changes in temperature are probably due to the effect of terrain variation on the slope of the sigma surface.

The cold air continues to penetrate southward for the next twelve hours reaching its maximum southward extent at 108 h (Fig. 17). At 24°N the minimum temperature is 298K, a -12K change from 84 h. The cold air does not penetrate much beyond the southern valley border. At 20°N the temperature change is approximately -2K in 24 h. While southward movement of the cold air ceases at 108 h, it does expand eastward, apparently in response to the eastward movement of the anticyclone located north of the valley. The cold air tongue does not dissipate as rapidly as the pressure ridge, and a pool of relatively cool air remains in the western valley region until the arrival of the next mid-latitude cyclone.

At the higher levels, sigma = 7/12 and 9/12, a small tongue of cold air forms between 78 and 84 h above the western valley wall. The southward extent is slightly less than that at the lowest level. As the low-level cold air tongue

moves rapidly southward after 84 h, the cold air at these
levels moves very slowly, only four degrees between 84 and
102 h at sigma = 7/12. Little, if any, eastward expansion
is seen. Beyond 108 h the very slight gradients are diffi-
cult to discern, primarily due to the increasing small scale
noise. At sigma = 9/12 the cold air more closely follows
the behavior of the cold air tongue at the lowest level
showing continued south and eastward expansion on the same
time scale, although of less intensity.

To verify that the changes in the potential temperature
fields at the upper-levels are essentially due to the use of
the sigma coordinate system, the temperature (T) fields were
analyzed at 850, 700 and 500 mb between 84 and 102 h. At
850 mb the intrusion of cold air can easily be traced. At
700 mb the cold air tongue is not discernable although this
may partially be due to the adiabatic warming effects appar-
ent at both the 700 and 850 mb levels. At 500 mb some small
scale noise is introduced by flow over and around the valley
but there is no evidence of the southward movement of cold
air. Therefore it is reasonable to assume that the changes
in the potential temperature fields at the higher levels are
due to the effect terrain variation has on the slope of the

sigma surface. The apparent movement of colder potential temperatures southward, then, is merely the result of the sigma surface being at a lower elevation in the valley region. To some extent this effect is seen near the eastern valley wall at the lower levels as well.

At 78 h, when the valley is only partially completed, a southward deflection of the northwesterly winds ahead of the ridge is readily apparent. By 84 h the valley is complete and the north winds are rapidly moving southward (Fig. 18). Along the valley wall the leading edge of the wind surge is highly ageostrophic. A strong southwesterly flow has set up in the eastern region of the valley presumably in response to the tight pressure gradient that exists there. It is interesting to note the small cyclone that has developed downwind of the western valley wall. It appears to be slightly better defined than the pre-existing low to the northeast and may result from the combined effects of the shear line and of cyclonic flow induced in the descending air by the conservation of potential vorticity. The cyclone dissipates as the north wind continues to push south and eastward into the valley. The shear line remains well defined between the opposing northerly and southwesterly

flows. The strong, cross-isobaric southwest winds in the eastern valley coincide with a very tight pressure gradient and may represent a sloping front in the valley.

At 96 h the north wind regime extends the length of the western valley wall and is spreading eastward across the valley (Fig. 19). At 102 h the north winds have reached their maximum extent; the wind regime occupies fully half the valley but does not extend south of it. The flow along the valley wall is no longer ageostrophic. The north winds entering the valley between 84 and 102 h are identifiable only at the very lowest levels, in agreement with the definition of a monsoon surge as a low-level phenomenon. By 108 h the anticyclone has moved sufficiently eastward that the light northerly winds associated with the ridge line have replaced the strong northwest flow previously located north of the valley (Fig. 20). The flow into the valley is greatly reduced and, without this support, the surge weakens and dissipates. The eastern region continues to be dominated by southwest flow.

It is clear that the movement of the north winds through the valley correlates well with the development of the cold air tongue and pressure ridge discussed earlier.

In summary, several observations can be made from the analysis of these fields. First, all three fields show the very rapid southward movement of a cold, high pressure airmass along the western valley wall between 84 and 96 h. Much slower southward movement continues through 108 h. Second, the airmass expands eastward across the valley in response to the continued eastward movement of the anticyclone. And third, the airmass never penetrates the tropical regions but remains within the confines of the valley.

C. EXPERIMENT 4

In this experiment the mountain range is again centered at 30°N. The valley, built between 72 and 84 h, is 24 grid-lengths wide, ie. two-thirds of the mountain range in length. The terrain then is actually the small east-west oriented mountain range displayed in Fig. 21. As in Experiment #3, the critical period for the surge is between 82 and 108 h while the anticyclone is located northwest of the valley.

The first 72 h of development are described by Control Run #2. As in the previous experiment the creation of the valley causes an oscillation in the pressure (ie. mass) field. The oscillation in this experiment is larger than

40

that of the previous case since the reduction of terrain is greater. The rapid increase in cyclogenesis also occurs earlier, supporting the assumption that the mountains exert a stabilizing influence on the disturbance.

At 84 h a small southward extension of the high pressure ridge can be seen over the eastern mountain slope (western valley wall). A low is centered over the northern valley with a weak trough extending southwest over the valley wall. A tight gradient develops south of the low, extending over the eastern valley wall and continuing along the northern mountain slopes. The trough is strongest at 78 h and is subsequently pushed southward by the expanding high pressure ridge. The ridge advances southward during the next twelve hours reaching the southern valley edge at 96 h (Fig. 22). Thus far movement of the ridge is quite similar to Experiment #3, although it does appear to be slightly weaker and not as readily discernable.

Between 96 and 108 h the mid-latitude ridge weakens considerably. Concurrently, a strong pressure gradient builds along the western edge of the ridge, in part due to a trough extending southward from the intense cyclone located to the northwest (Fig. 23). A similar gradient is seen during the

41

same period in Experiment #3 but is not nearly as intense. At both 102 and 108 h there is evidence that the ridge extends slightly beyond the edge of the valley.

The development and movement of the ridge agrees very closely with that of the earlier experiment using a smaller valley. In both cases the ridge begins development while the valley is growing, moves southward along the western wall at the same rate, reaches the southern edge at the 96 h point and weakens when the anticyclone moves to a location due north of the valley. There is, however, a slight difference in intensity. The third experiment shows a well defined, easily discernable ridge from 84 to 108 h. In the present experiment the gradient along the western side of the ridge is greater, but the ridge itself is not as well defined.

A weak tongue of cold air can be seen along the western valley wall at 84 h (Fig. 24). An increase in the temperature gradient is apparent in the extreme western valley at the lower three levels although it is very weak at the uppermost of these (sigma = 7/12). These levels correspond to pressure heights lower than 600 mbs in a standard atmosphere. Through the next twelve hours the cold air tongue

moves southward and strengthens. By 96 h the cold air has reached the southern edge of the valley (Fig. 25). The cold air tongue is much better defined than the pressure ridge. It is nearly identical to the cold air tongue seen in the western valley for Experiment #3. The minimum temperature at 24°N has fallen from 310K at 84 h to 300K at 96 h. The temperature change is primarily limited to the western third of the valley, temperatures in the eastern two-thirds have remained relatively constant following completion of the valley.

The cold air continues to move south and eastward through the next twelve hours. Maximum southward extent is reached at 108 h. At 24°N the minimum temperature is 298K and represents the same change in temperature, -12K, as was seen in Experiment #3 (Fig. 26). While southward movement of the cold air has ceased, it does continue to expand eastward well past this time. The primary axis of the cold air tongue remains along the western valley wall and retains its identity through 120 h. A pool of cool air remains in the western valley for another twelve hours. At sigma = 9/12 the cold air is discernable well past 108 h. At higher levels the small scale noise has more effect and the cold air is difficult to trace past this time.

43

The upper-levels display the same behavior seen in Experiment #3. A slight increase in eastward expansion at these levels is seen, possibly due to the much wider valley.

As with the pressure and temperature fields the development of the north wind surge in this experiment closely follows that of Experiment #3. At 84 h the north winds have reached mid-valley and continue to spread rapidly southward. Again the leading edge of the wind surge is ageostrophic. A strong southwesterly flow has set up in the valley apparently due to the tight pressure gradient located there (Fig. 27). The small cyclones seen in Experiment #3 are not apparent here although cyclonic flow exists, possibly due to the convergence of the southwest flow from the tropics and the opposing flow out of the mid-latitude anticylones. This cyclonic flow weakens considerably after 84 h.

At 96 h the north wind regime extends almost the entire length of the valley and is spreading eastward. The southward extent of the north winds along the valley wall is identical to that of Experiemtn #3 (Fig. 28). Further east the perimeter of the north wind regime is nearly two degrees farther south of that reached in the earlier experiment. The mid-latitude ridge weakens during the next six hours,

and with its continued eastward movement, results in a decrease in the northwesterly winds supporting the surge. Thus only a very little southward movement takes place between 96 and 102 h, the time of maximum southward extent of the north winds. The ageostrophic component of the flow weakens rapidly as southward movement along the valley wall slows. The winds become much weaker but do not decrease in coverage through 108 h (Fig. 29). A slight eastward movement is seen as the ridge moves past the mountains and north of the valley. After 108 h the north winds diminish and move eastward in response to the weakening and continued eastward movement of the ridge. After 120 h the wind surge is no longer discernable.

The surge is identifiable only at the two lowest levels. At sigma = 9/12 the surge is weaker and less extensive than at the lowest level. It dissipates very rapidly after 102 h as the ridge at this level moves north of the valley.

In this experiment a slight increase in the eastward extent of the north winds is noted when compared to Experiment #3. Since topography is the only parameter changed, it is reasonable to assume the increase in eastward extent is a result of the expanded valley. It should be noted though

that while the valley size has doubled, the corresponding
increase in longitudinal coverage by the north winds is
extremely small.

Several observations can be made from the results of
Experiment #4. First, all three fields show the rapid
southward movement of the cold, high pressure airmass along
the western valley wall between 84 and 96 h. Subsequent
southward expansion is much slower. Second, the airmass
expands eastward across the valley in response to the east-
ward movement of the anticyclone. And third, there is a
tendancy towards cooling and rising pressures just south of
the valley although the north winds remain within the valley
confines.

D. EXPERIMENT 5

In this experiment the mountain range is centered at
38°N, eight degrees farther north than in previous experi-
ments. The valley is twelve gridlengths wide, as in Experi-
ment #3. Terrain is shown in Fig. 30. Cyclogenesis is
considerably slower than that seen in either of Experiments
3 or 4. This is due to the placement of the northern moun-
tain slopes at the same latitude as the maximum amplitude of
the disturbance. Growth of the perturbation is prevented by

effectively blocking the north-south heat flux. For this reason the initiation of valley growth was delayed six hours to allow additional time for development of the disturbance. The growth period for the valley is now between 78 and 90 h. As with the previous experiments the creation of the valley causes an oscillation in the pressure field, the approximate amplitude of that in Experiment #3.

At 90 h a strong low is located in the northeast of the valley trough extending southwest over the valley wall. This results in a tight pressure gradient in the eastern valley and along the northern mountain slopes similar to the gradients found in previous experiments. The mid-latitude anticyclone is neither as strong nor as well developed as in Experiments 3 and 4, and although there does appear to be a slight southward extension of the high pressure along the western valley wall, it is very weak. During the next twelve hours a ridge of high pressure builds along the valley wall, however it is difficult to determine whether the high pressure originates in the anticyclone to the northwest or in the tropical regions south of the valley (Fig. 31). As the analysis of the wind fields will later show, the high pressure air does originate in the mid-latitude anticyclone.

47

At 102 h the anticyclone is ill-defined and the mountain region to its south populated by small high and low centers.

Between 102 and 114 h the ridge moves east into the valley and strengthens, this is particularily noticeable at 114 h (Fig. 32). It appears the anticyclone has slipped beneath the cyclone and is re-forming in the northern valley. During this time a weak trough can be seen forming over the northwestern valley wall.

At 120 h the anticyclone is located in the northeast valley region with a weak ridge extending southwest through the valley and a stronger, better defined ridge to the northwest. Low pressures are found over the western valley wall due to a weak trough forming ahead of the mid-latitude cyclone.

In earlier experiments the high pressure ridge developed and strengthened along the western valley wall only to dissipate as the anticyclone moved to a position northeast of the ridge. In this experiment the ridge is weaker, not well-defined and moves eastward with the anticyclone. Since the northern valley is located at the latitude of maximum amplitude for the disturbance, creating the valley allows the anticyclone to reform in this area as the weak ridge

moves eastward into the valley. The same reasoning can be used to explain the strong development experienced by the low during the valley growth period; it was located along the northern mountain slopes at the same longitude as the valley.

A weak tongue of cold air can be seen along the western valley wall at 90 h (Fig. 33). This gradient is found in the lowest three levels, weakening with height. At the upper-levels (sigma = 5/12, 3/12, 1/12) nearly identical gradients exist at both ends of the valley and are due to the effects of terrain on the slope of sigma surfaces. The cold air tongue strengthens and moves rapidly southward in the following six hours. By 102 h the cold air has reached the southern edge of the valley (Fig. 34). The development and movement of the cold air tongue is much better defined than that of the pressure ridge. It is nearly identical in development and intensity to the cold air tongues seen in Experiments 3 and 4. The minimum temperature at 32°N (a comparable latitude to 24°N relative to the position of the mountains) is 295K compared to 306K at 90 h. This is a temperature change of -11K compared to -12K and -10K for Experiments 3 and 4 respectively. Again the temperature

49

change is primarily limited to the western third of the valley.

The cold air continues to move south and eastward during the next twelve hours, reaching its maximum southward extent at 114 h (Fig. 35). At 32°N the minimum temperature is 293K, a temperature change of -13K compared to -12K in Experiments 3 and 4 for a 24-h period following completion of the valley. Eastward expansion of the cold air continues past 114 h. In the previous experiments the axis of the cold air tongue remained along the western valley wall. In this experiment the cold air moves eastward as well, particularily in the northwest region. This is probably the result of the anticyclone reforming in the northern valley and the subsequent eastward movement of the pressure ridge. The cold air tongue does not move as far eastward as the ridge and begins to weaken when the anticyclone moves northeast of the valley.

The upper-levels display the same behavior seen in Experiments 3 and 4. A very slight movement of the northern portion of the cold air axis is seen at sigma = 9/12, but no similar movement is seen at sigma = 7/12. The increased small scale noise at these levels makes analysis of the

temperature fields difficult past 114 h. The highest levels (sigma = 5/12 to 1/12) show no sign of southward movement of cold air at any time.

As in the previous experiments southward deflection of the northwest winds into the valley occurs before the valley is completed. By 90 h the north winds have reached mid-valley with a shear line developing over the valley floor in advance of the northerly flow. North winds along the valley wall are strongly ageostrophic. Again a strong southwest flow has set up in response to the tight pressure gradient in the eastern valley. Although the valley is the same as that used in Experiment #3, the subsequent pattern of development is slightly different. At 96 h the northwest winds reach the eastern valley wall, whereas, in Experiment #3 the strong southwest flow in this region prevents the northwest winds from spanning the valley. The wind surge is actually strongest at this time, and has its greatest southward extent (Fig. 36). By 102 h the ridge is north of the valley wall and the winds are beginning to weaken, the flow is no longer ageostrophic. The north winds never reach the southern edge of the valley (Fig. 37). The surge continues to weaken rapidly and at 108 h the anticyclone is reforming

51

within the valley.   North winds exist in the central valley region but do not coincide with the position of the cold, high pressure ridge.   Six hours later the anticyclone is established over the north central valley and no evidence of the surge exists (Fig. 38).   It is clear that positioning the mountain range at 38°N has a detrimental effect on the development of the surge.

The surge is identifiable at only the two lowest levels. At sigma = 9/12 the surge is less extensive and weaker than at the lowest level.   At sigma = 7/12 and 5/12 a weak cyclonic turning of the winds is apparent but no definite southward flow can be seen.   The cyclonic flow disappears as the anticyclone reforms over the valley.

In summary the following observations can be made from this experiment.   First, all three fields show the rapid southward movement of cold, high pressure air along the western valley wall during the first six hours following valley completion.   Second, the movement and development of the cold air tongue is much better defined than that of the pressure ridge and wind surge, both of which weaken considerably after 102 h.   Third, the pressure ridge and wind surge axis move eastward off the valley wall due to the

development of the anticyclone within the valley, only the northern most portion of the cold air tongue moves eastward. And fourth, although there is a slight cooling and pressure rise south of the valley, the north winds remain well within the valley.

E.   EXPERIMENTS 6 AND 7

The valley was included as part of the initial terrain configuration for these two experiments. The mountains are centered at 30°N and the valley is eight gridlengths wide, approximately one-quarter the length of the mountain range. This is the original mountain-valley configuration used with the model, the larger valley was used in subsequent runs to avoid interference between the strong southwesterly flow in the eastern valley and developing southward flow in the west. The southward movement of a cold, high pressure air-mass occurs with both valley sizes, however the airmass is more easily seen, and so more easily analyzed, with the larger valley.

Only the mean flow is initialized in Experiment #6. The purpose of this run is to confirm the assumption that the monsoon surge, if it occurs, is due to baroclinic wave and not a result of the interaction of the mean flow with the terrain.

53

As expected no "surge" occurs. The current that does form in the valley is southwesterly, flowing from high to low pressures. The strong southwesterly flow seen in Experiments 3 through 5 is in part due to the mean pressure gradient that exists between the northern and southern valley borders. By 30 h a small cyclone has formed over the western valley wall, probably due to the conservation of potential vorticity. This indicates that the small cyclone seen here and in other experiments is a result of the mean flow interacting with the terrain.

Experiment #7 is initialized with the perturbation. During the first portion of the experiment, while the disturbance is weak, southwesterly flow forms in the valley in response to the existing north-south pressure gradient. Again at 30 h a small cyclone has formed over the western valley wall. During the next twelve hours the center of the cyclone moves over the valley floor although the north winds remain located over the valley wall. The mid-latitude disturbance continues to strengthen and by 66 h the northerly winds are being enhanced by the northwest flow ahead of the approaching ridge. The northerly flow strengthens as the ridge moves eastward, at 96 h it extends slightly beyond the

valley edge, however this is its maximum southward extent. Subsequently the mid-latitude ridge axis moves north of the valley and the supporting northwest flow diminishes. The flow along the valley wall is never ageostrophic during this time.

The cyclone is readily apparent in the sea-level pressure fields. However, not until the ridge approaches the valley does a high pressure ridge build along the valley wall (72 h). The ridge weakens as the anticyclone moves to a position north of the valley.

The potential temperature field shows very little cooling along the western valley wall compared to previous experiments. Minimum temperature along 24°N at 90 h is 299K compared to 303K at 66 h, a decrease of only 4K in 24 h. A very small temperature change when compared to Experiments 3 through 5.
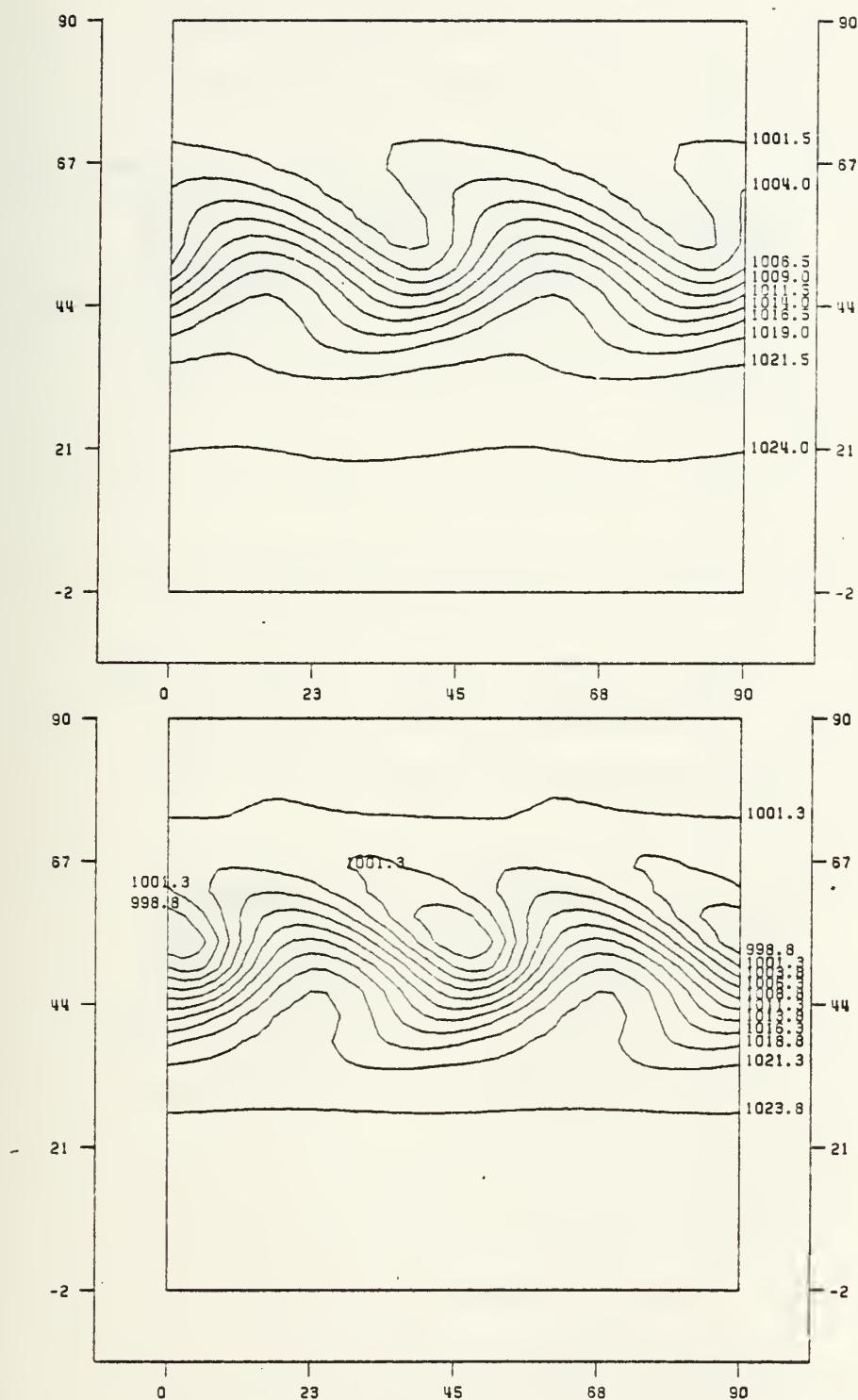
Figure 3. Sea-Level Pressure, 60 and 72 h, Exp. 1.

56
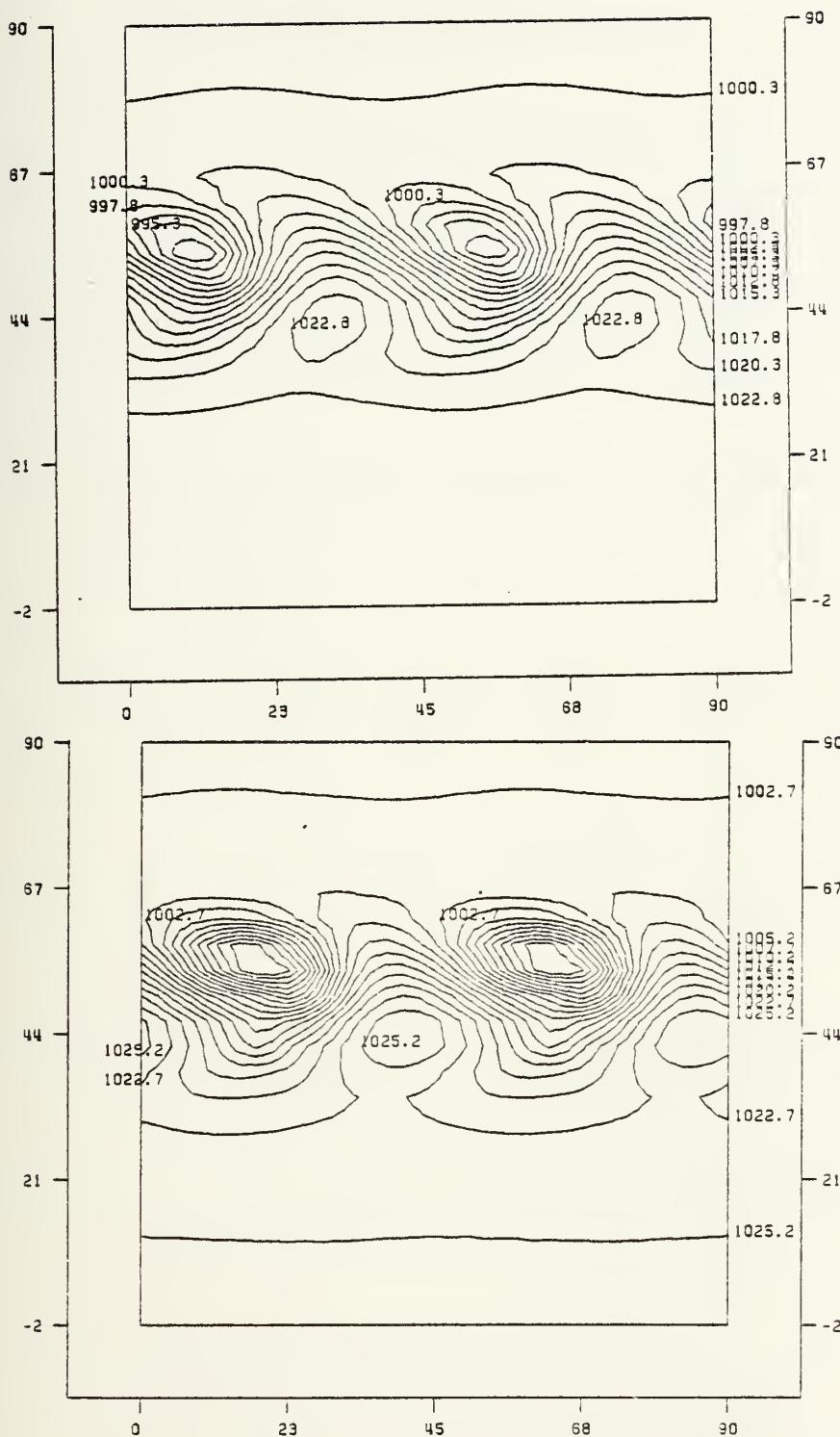
Figure 4. Sea-Level Pressure, 84 and 96 h, Exp. 1.

57
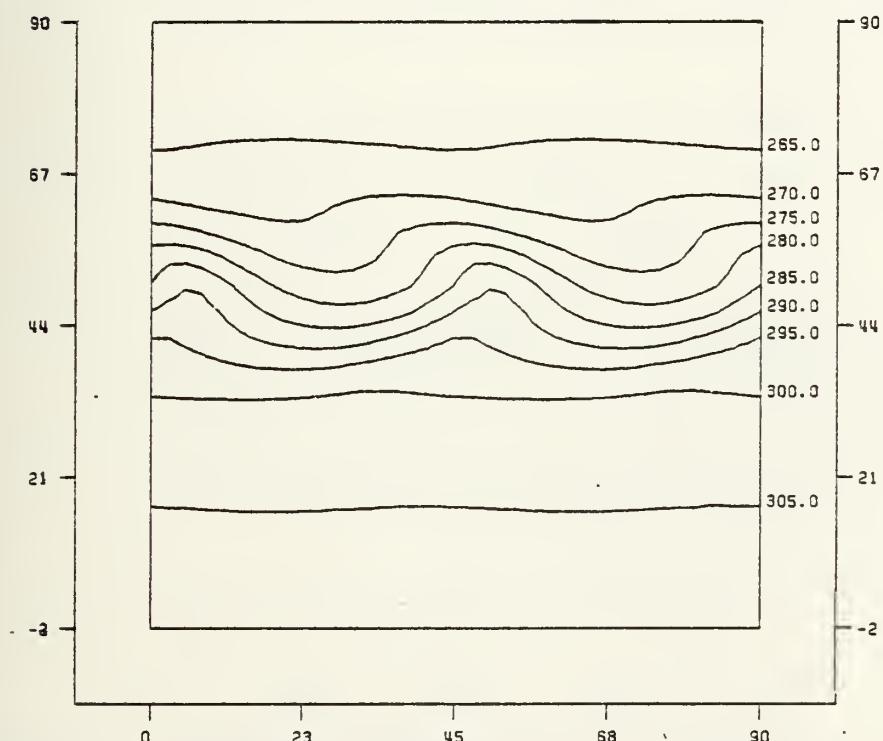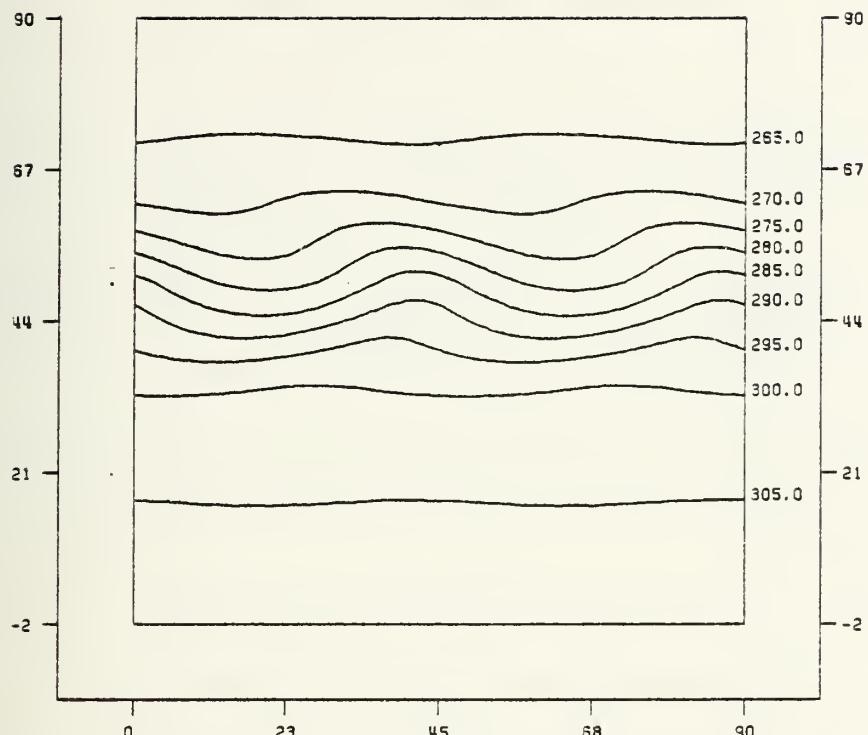
Figure 5.   Potential Temperature, 60 and 72 h, Exp. 1.
Sigma = 11/12.

58
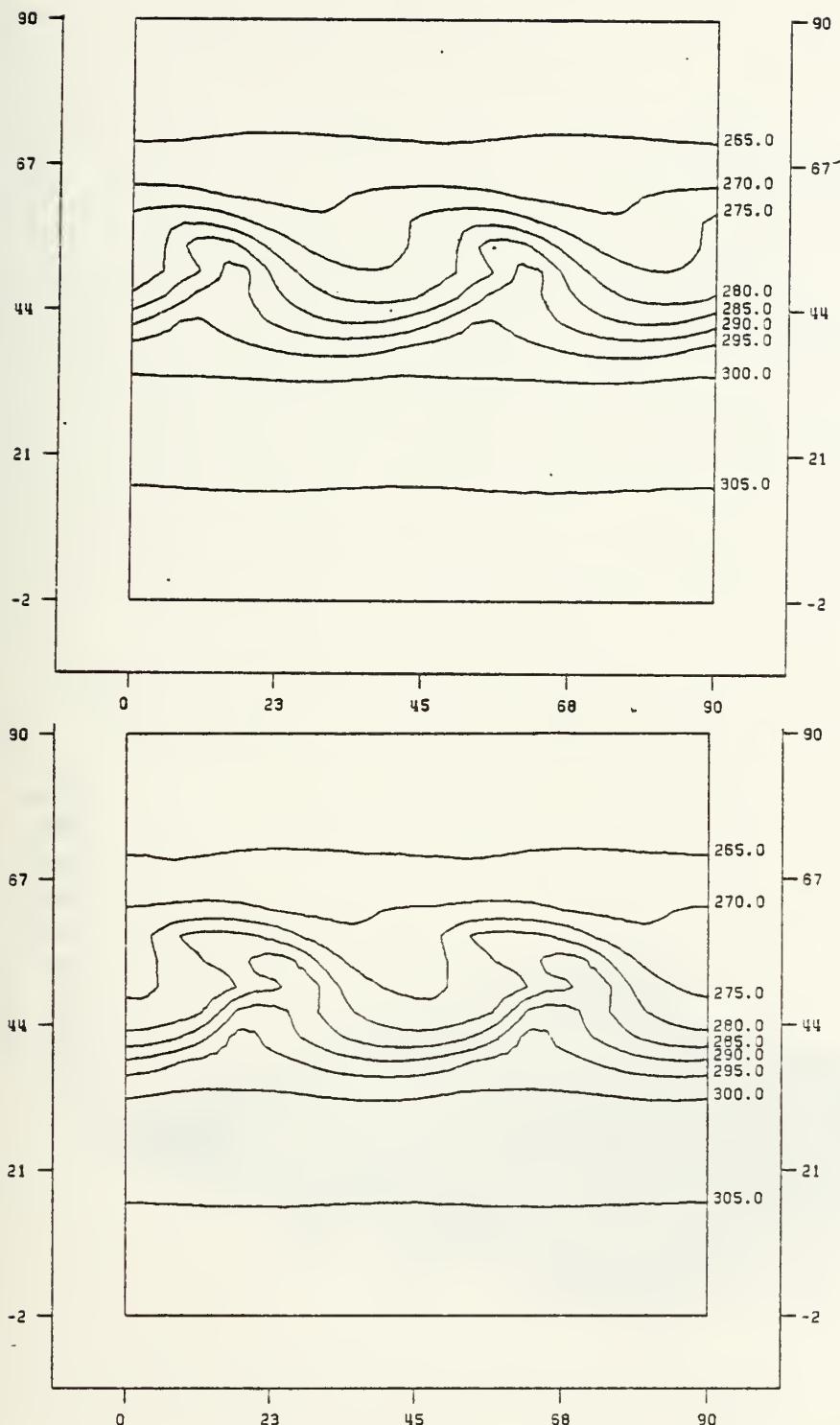
Figure 6. Potential Temperature, 84 and 96 h, Exp. 1. Sigma = 11/12.

59
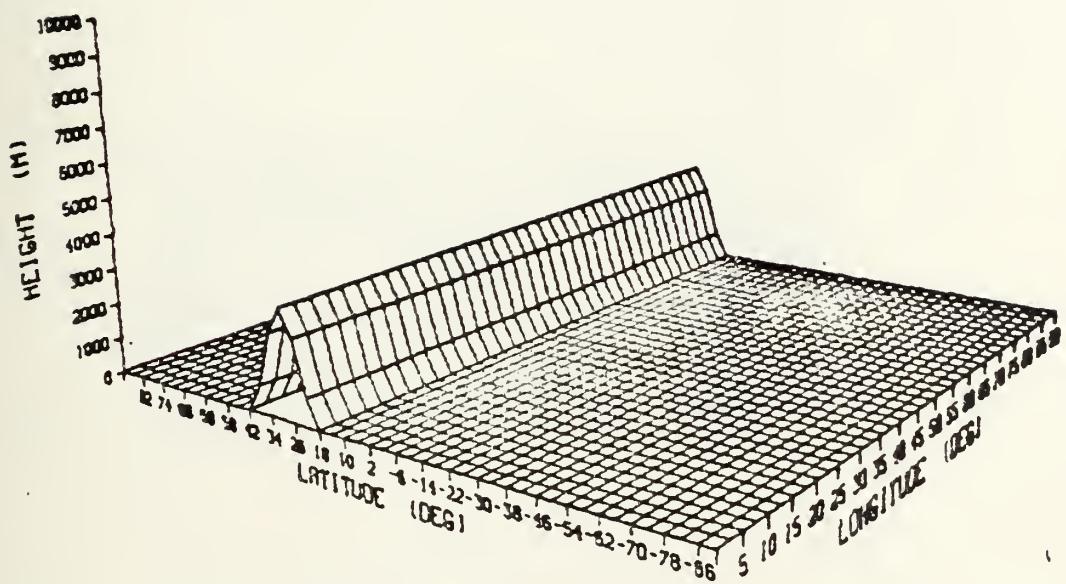
Figure 7. Model Terrain, Experiment 2.
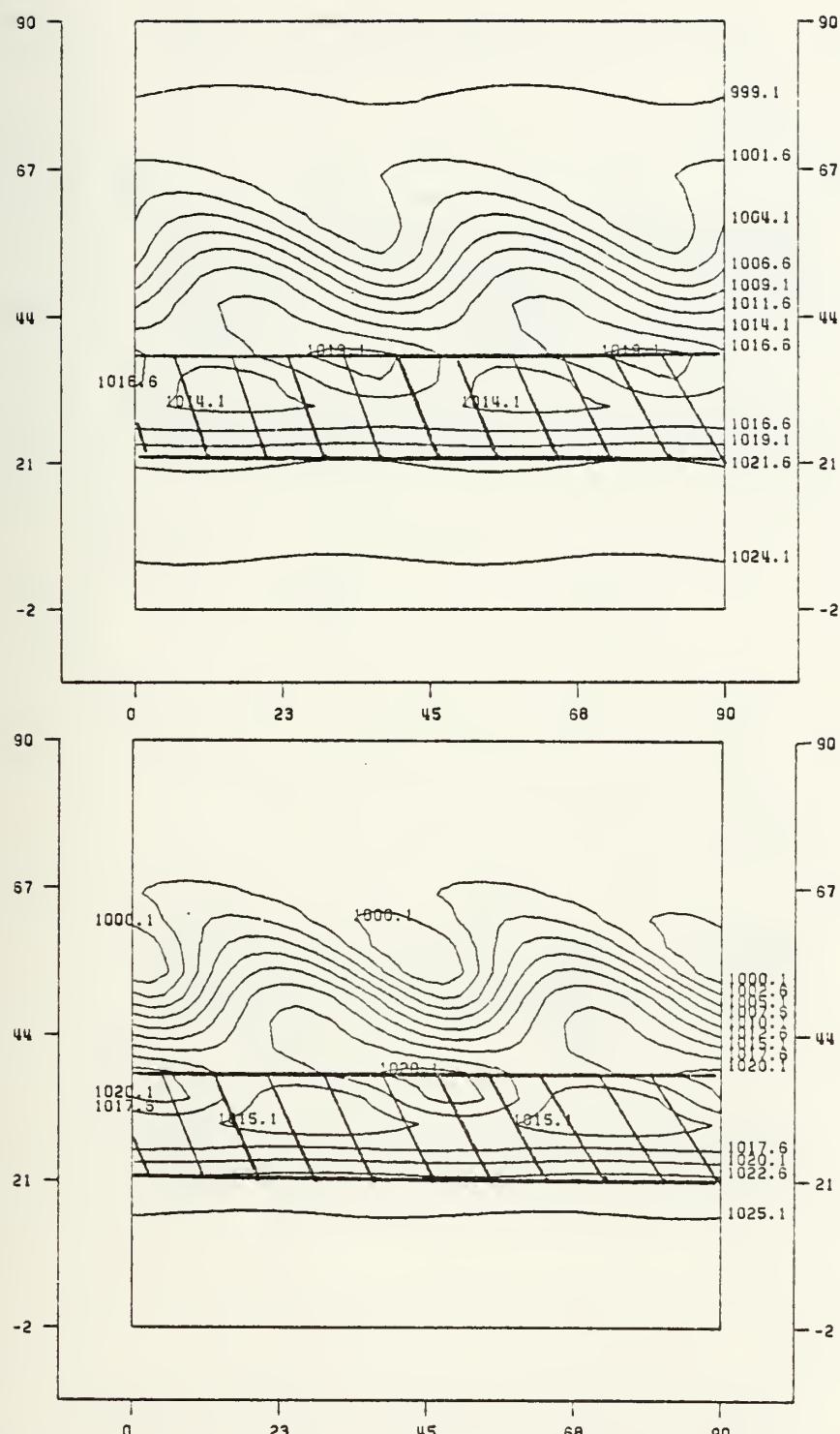
Figure 8. Sea-Level Pressure, 60 and 72 h, Exp. 2.

61
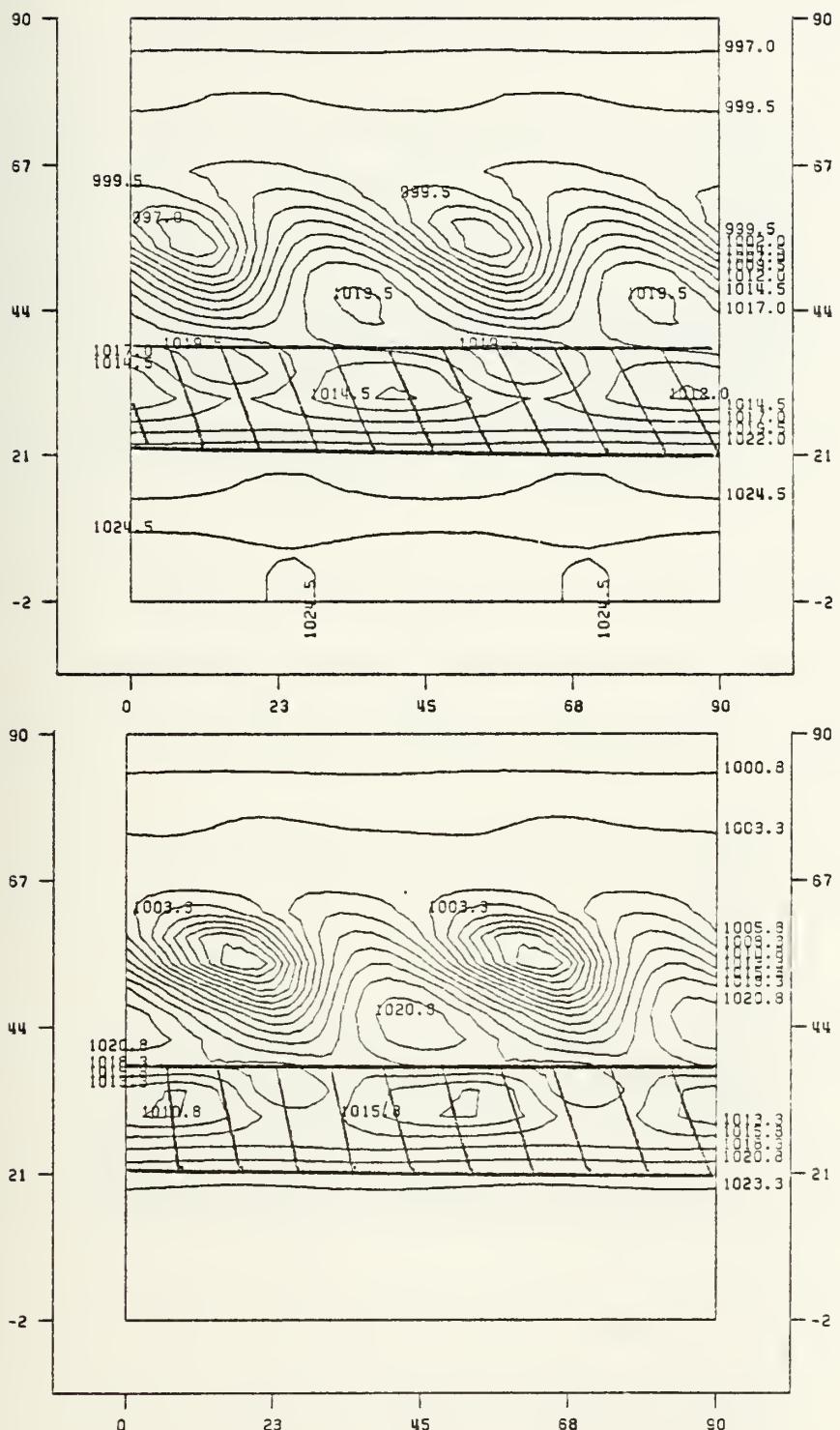
Figure 9. Sea-Level Pressure, 84 and 96 h, Exp. 2.
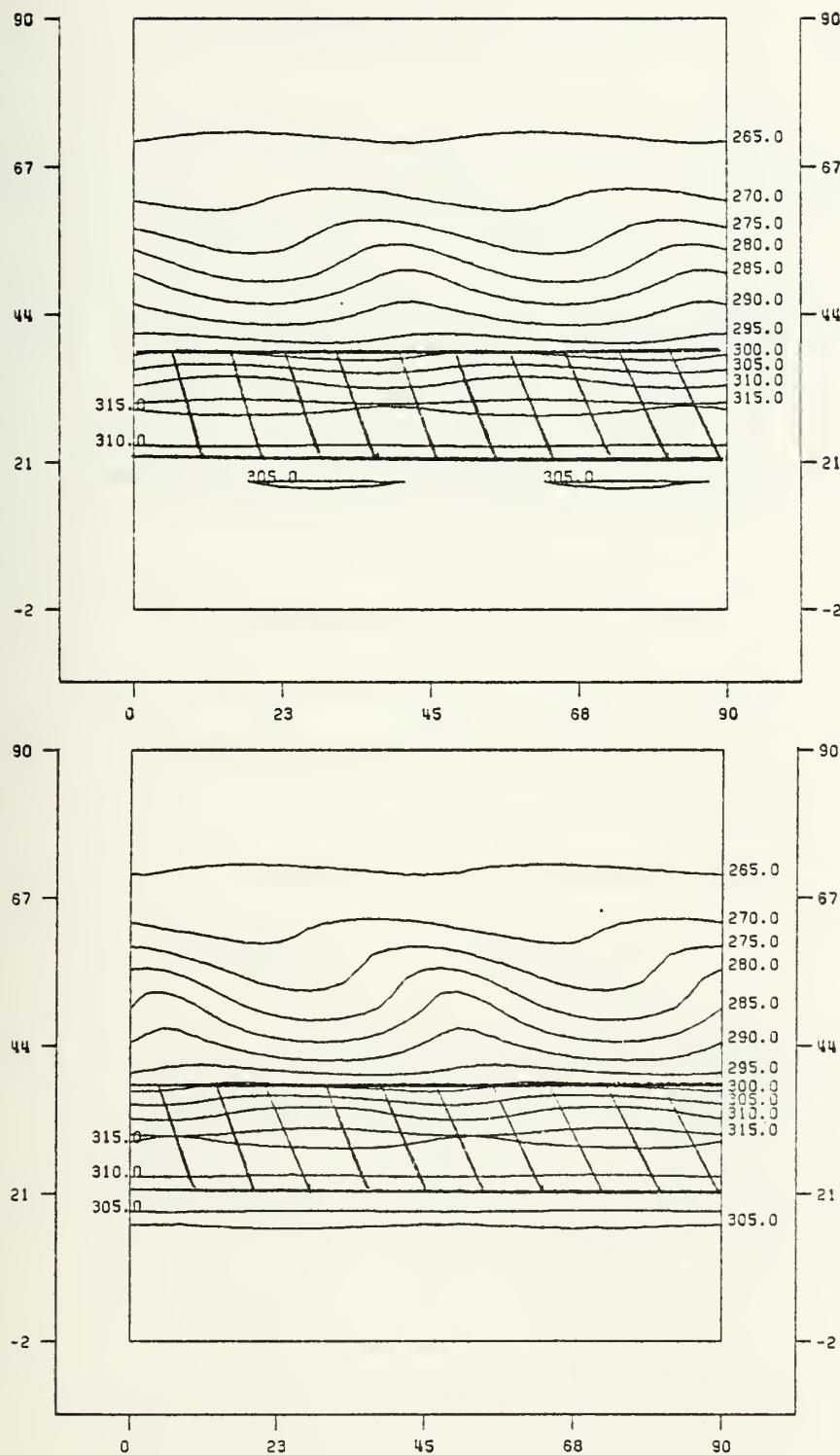
Figure 10.   Potential Temperature, 60 and 72 h, Exp. 2.
              Sigma = 11/12.

63
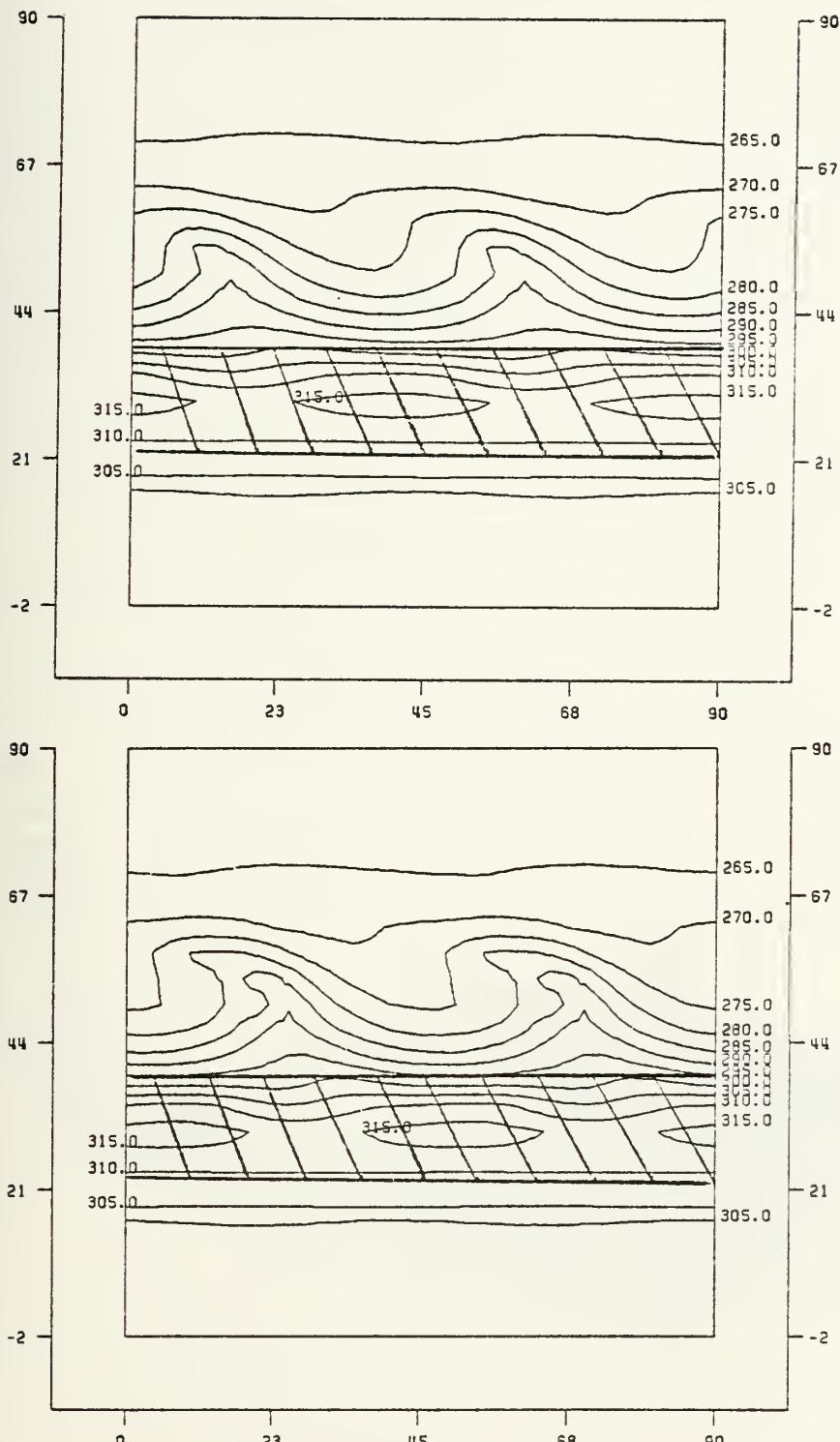
Figure 11. Potential Temperature, 84 and 96 h, Exp. 2. Sigma = 11/12.
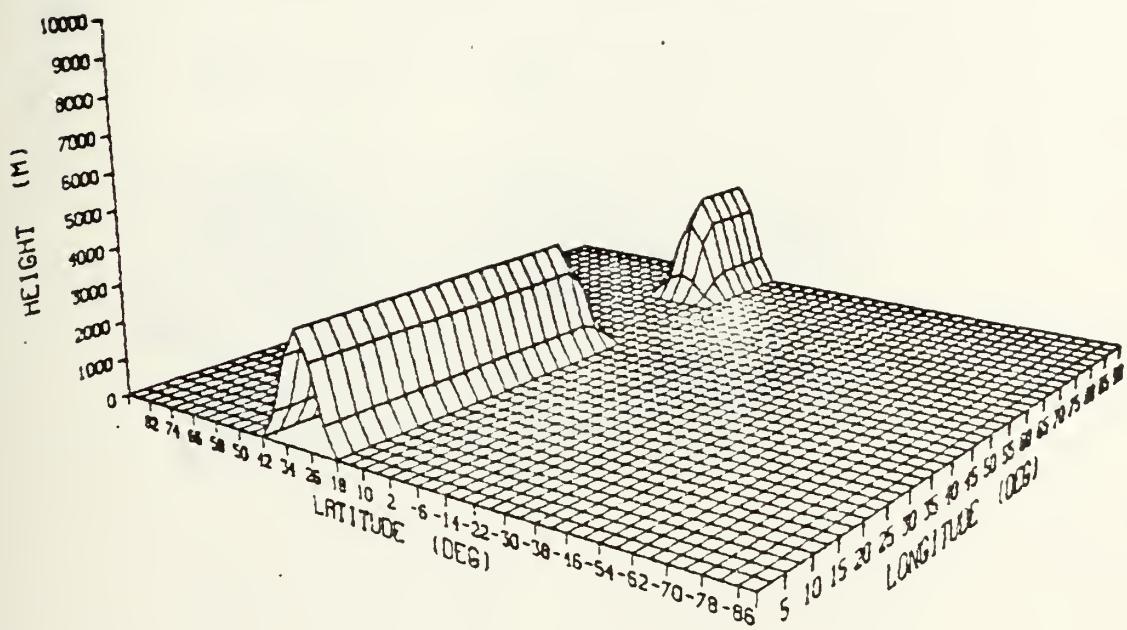
Figure 12. Model Terrain, Experiment 3.

65
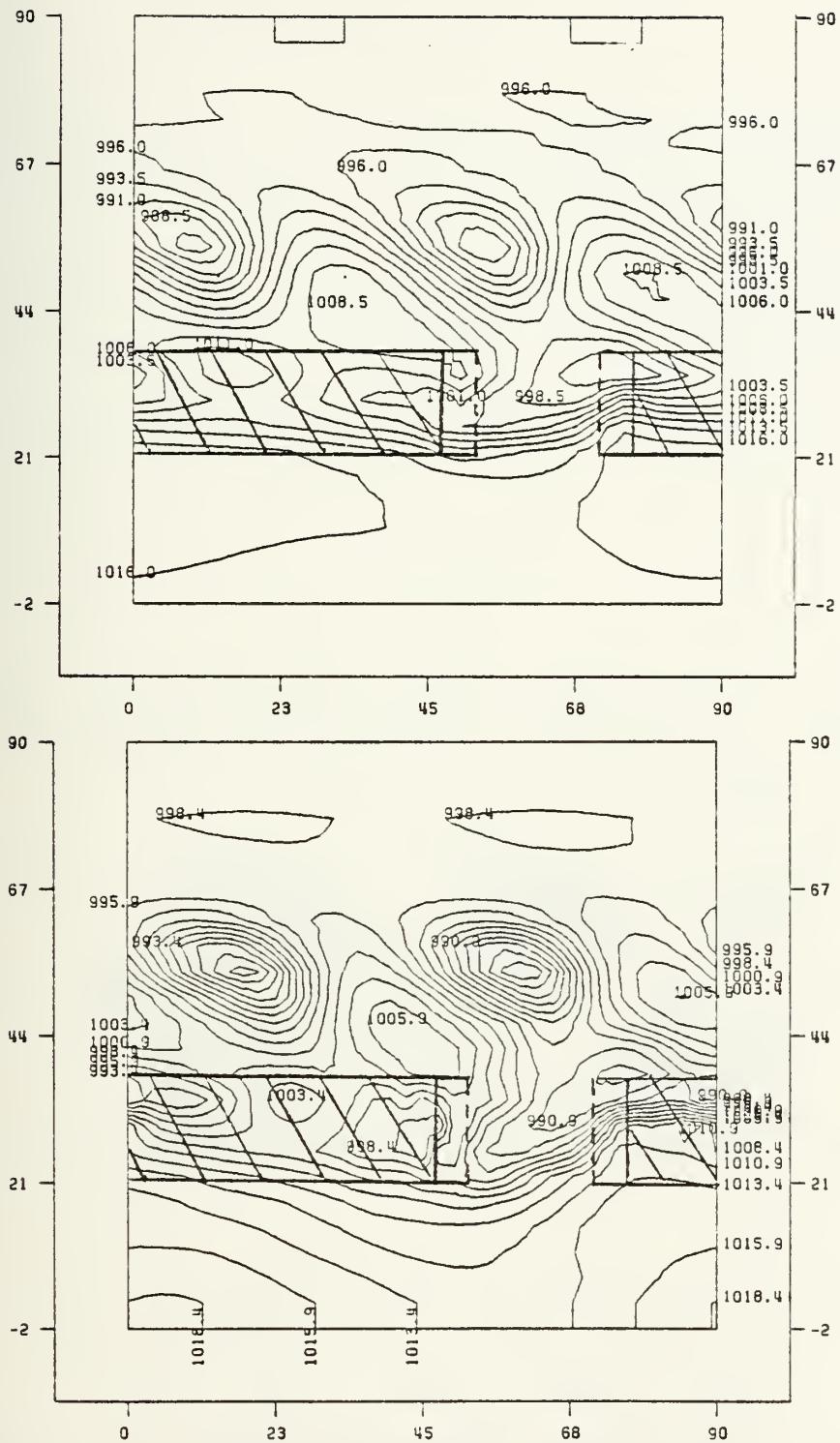
Figure 13.   Sea-Level Pressure, 84 and 96 h, Exp. 3.

66
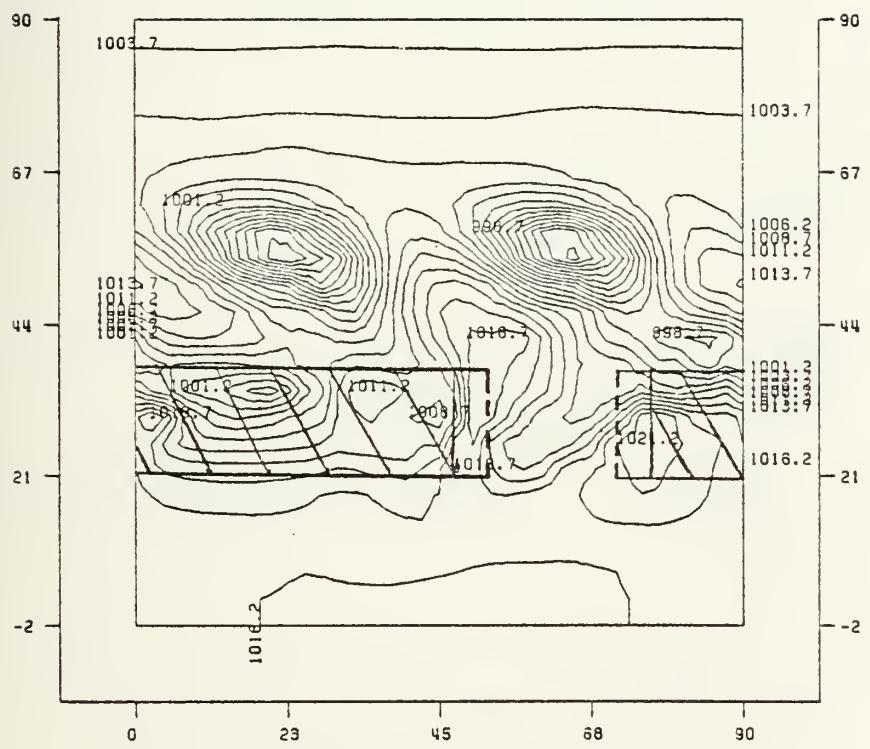
Figure 14.   Sea-Level Pressure, 108 h, Exp. 3.
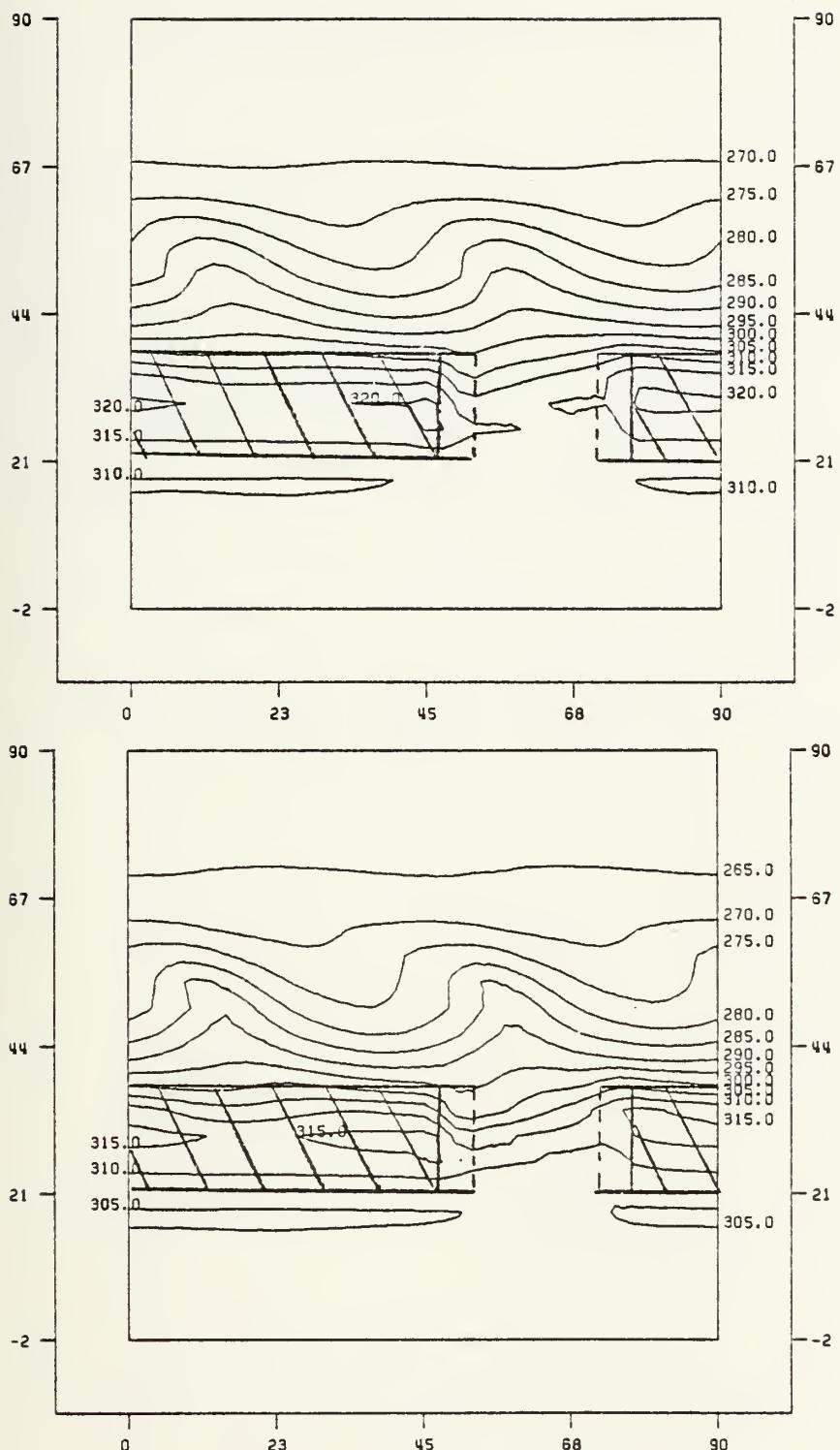
Figure 15.   Potential Temperature, 84 h, Exp. 3.   Sigma = 9/12, 11/12.
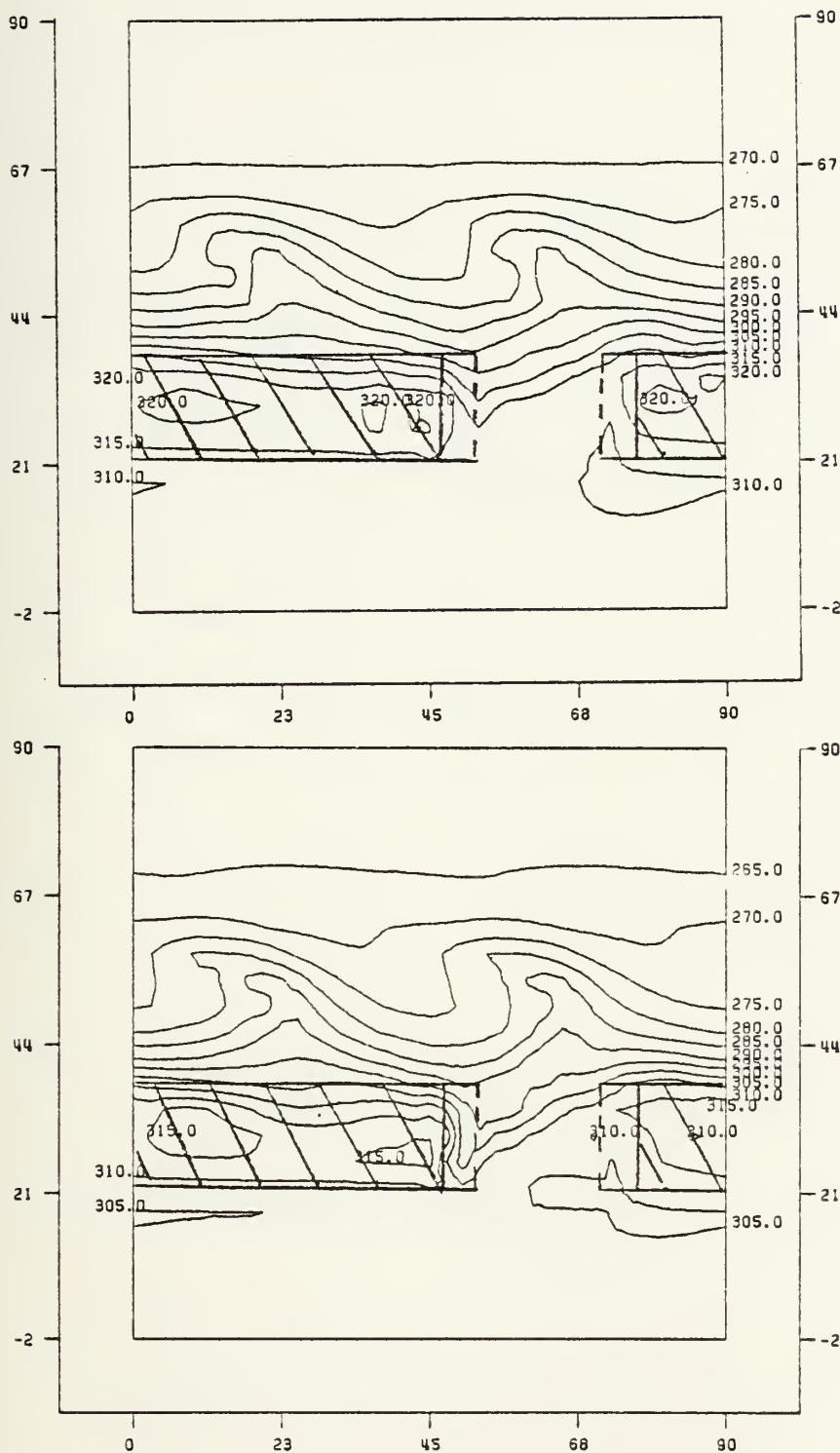
Figure 16. Potential Temperature, 96 h, Exp. 3. Sigma = 9/12, 11/12.
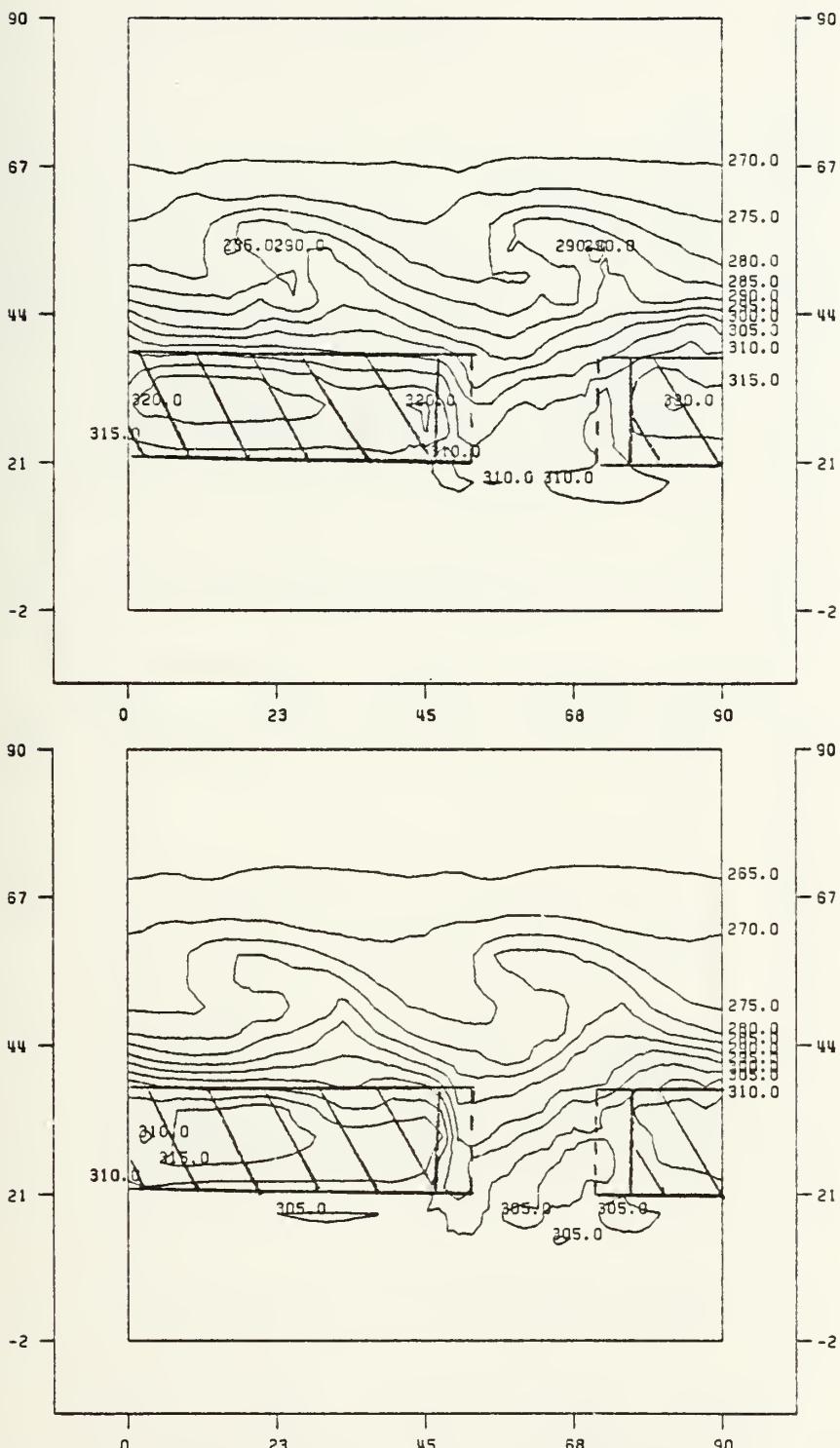
Figure 17.   Potential Temperature, 108 h, Exp. 3.   Sigma =
9/12, 11/12.
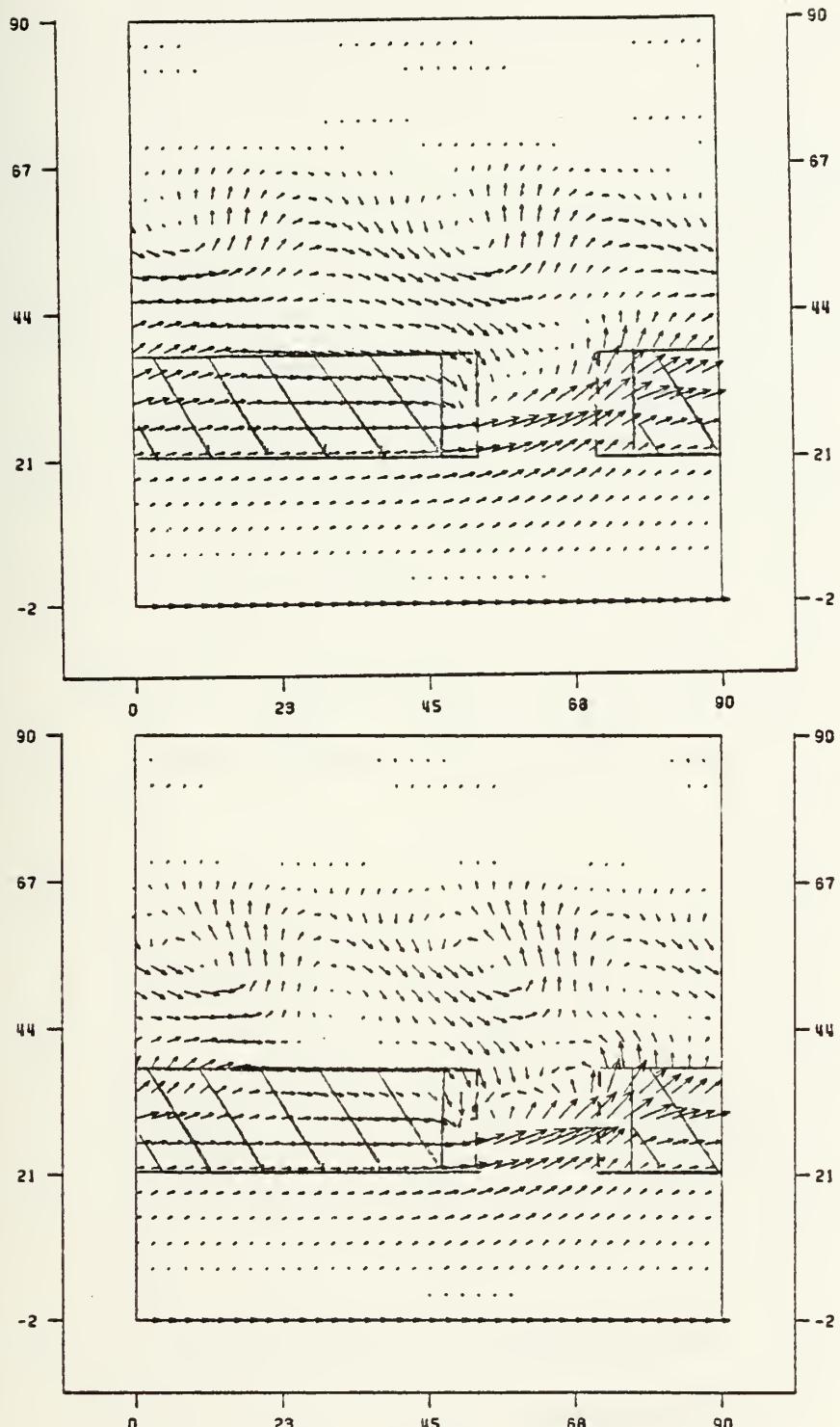
Figure 18.   Wind Vectors, 84 h, Experiment 3.   Sigma = 9/12, 11/12.
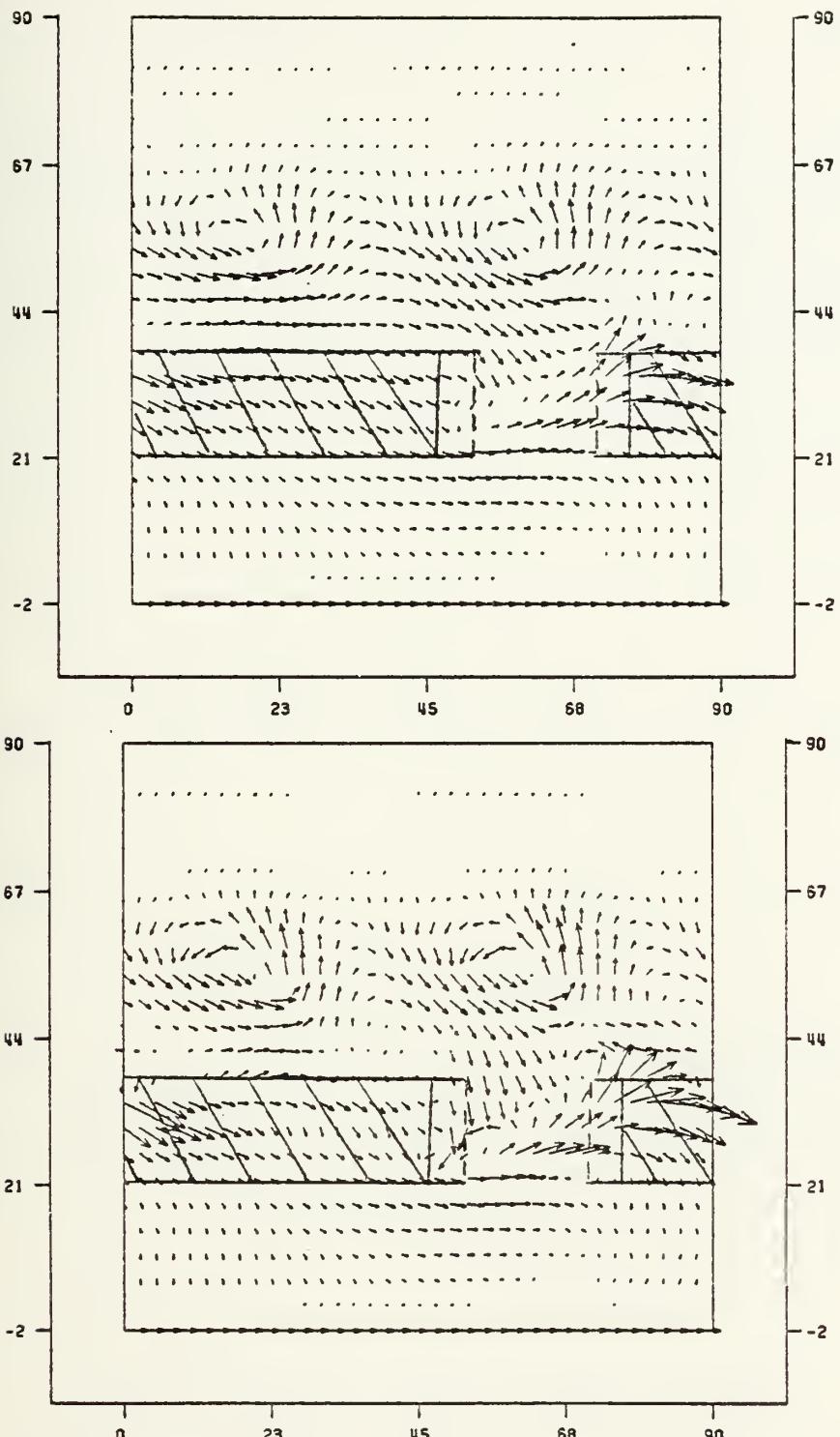
Figure 19.   Wind Vectors, 96 h, Experiment 3.   Sigma = 9/12, 11/12.

72
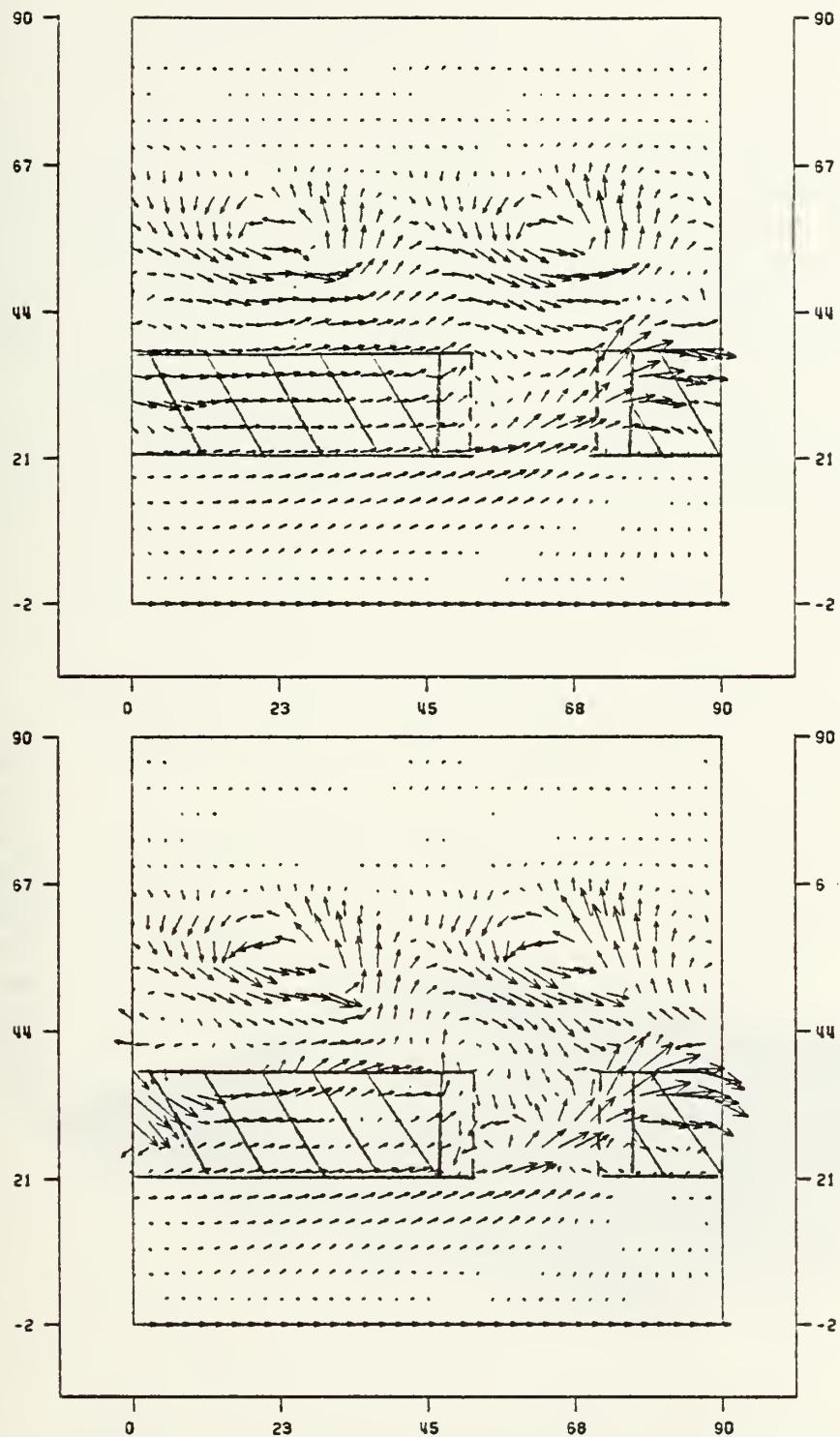
Figure 20. Wind Vectors, 108 h, Experiment 3. Sigma = 9/12, 11/12.
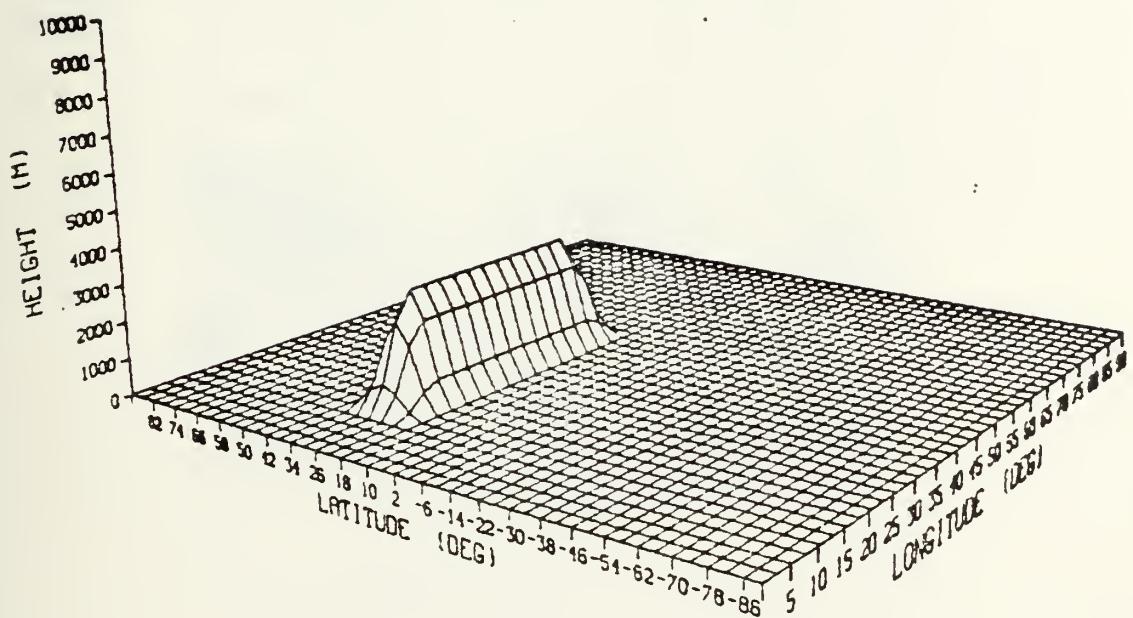
Figure 21. Model Terrain, Experiment 4.

74
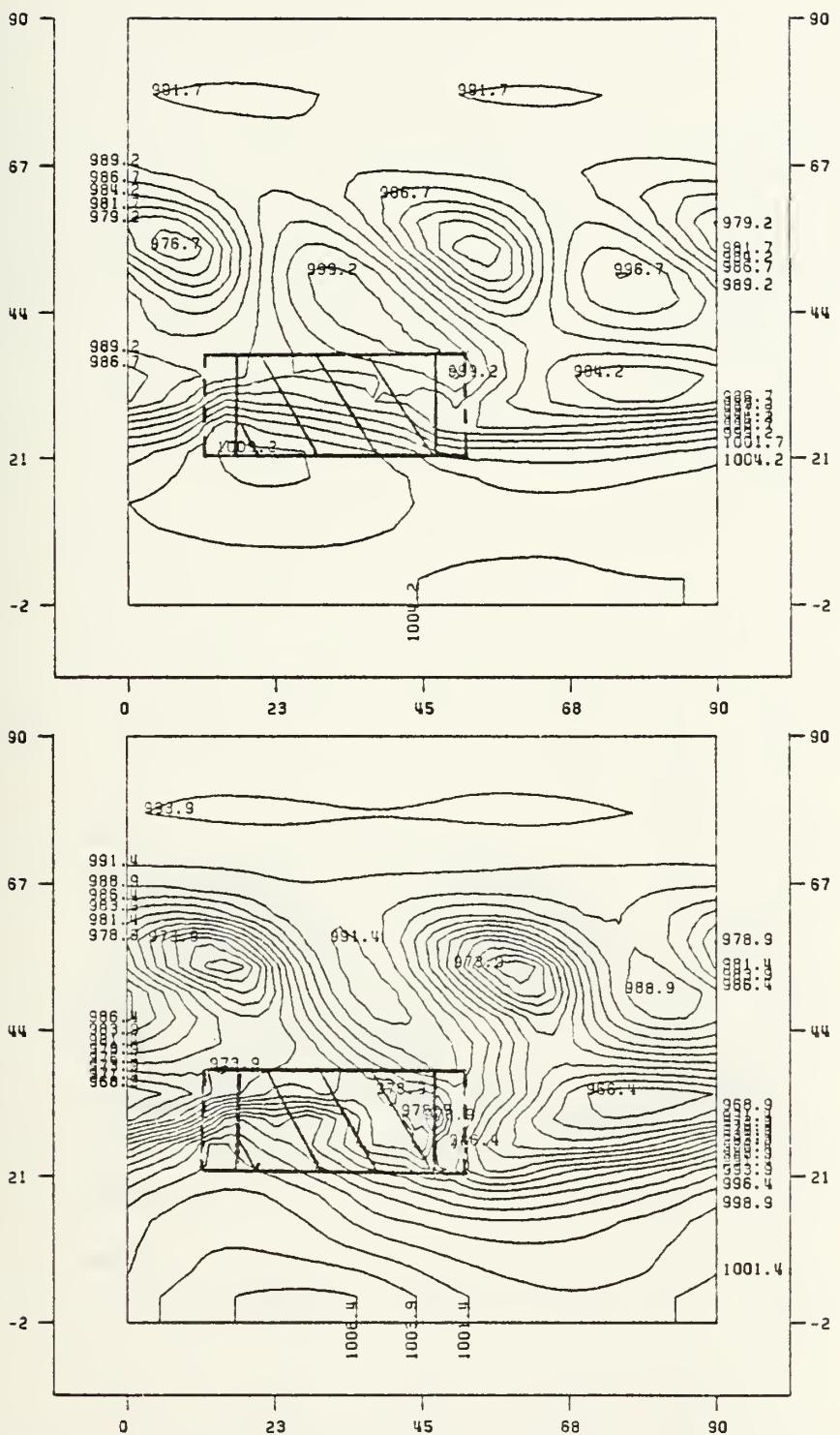
Figure 22.   Sea-Level Pressure, 84 and 96 h, Exp. 4.

75
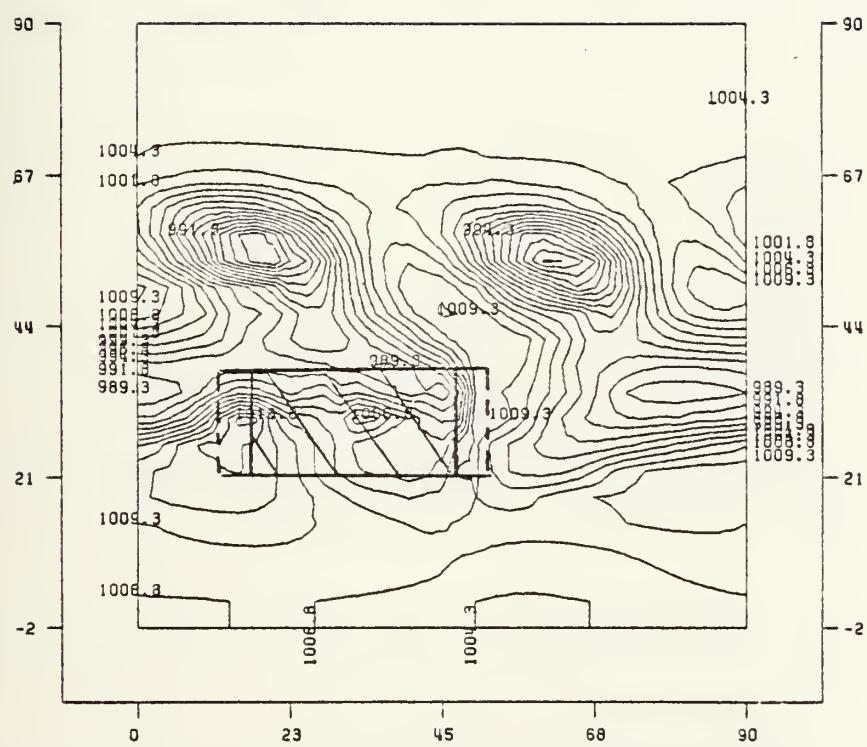
Figure 23.   Sea-Level Pressure, 108 h, Exp. 4.

76
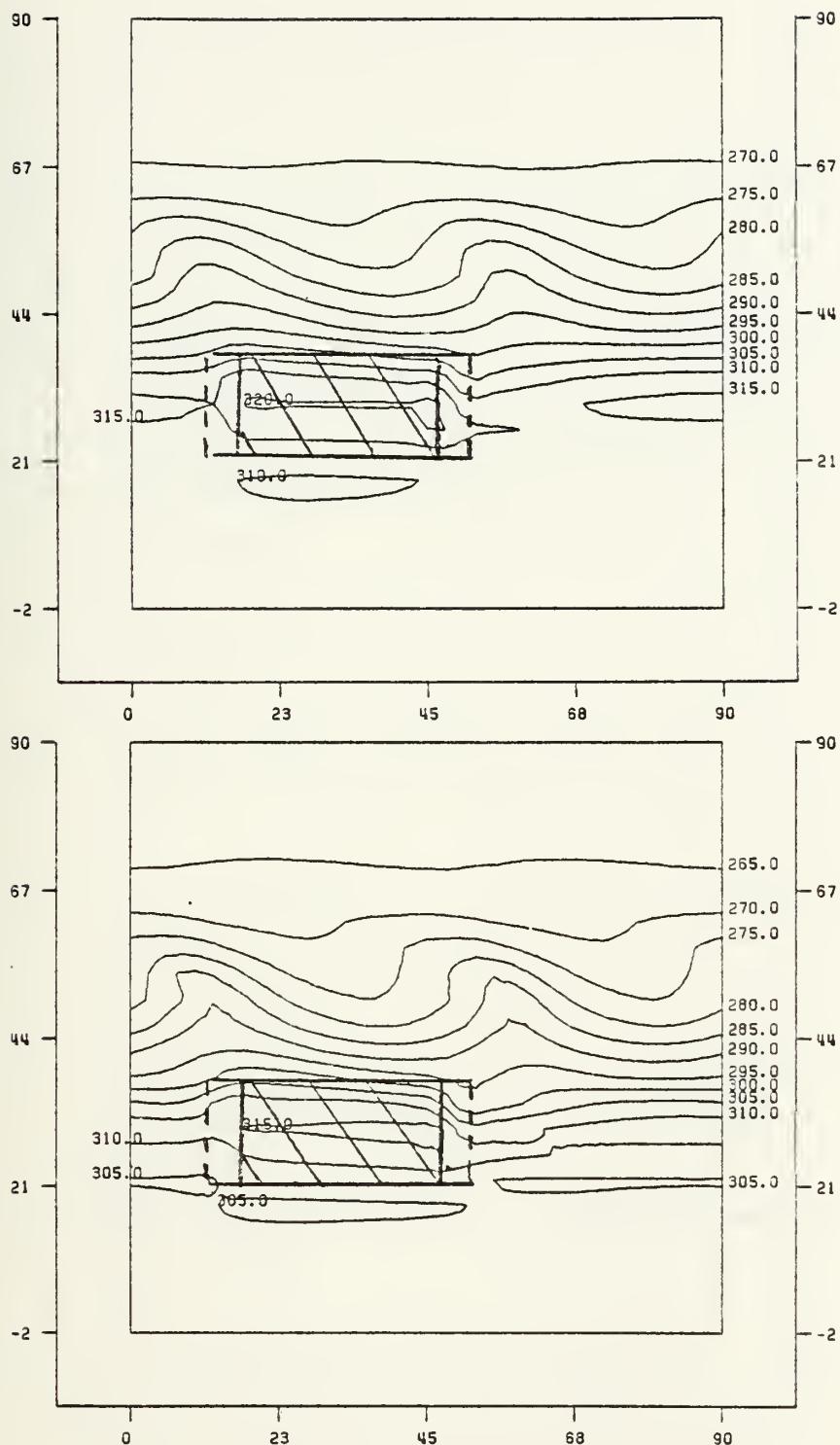
Figure 24. Potential Temperature, 84 h, Exp. 4. Sigma = 9/12, 11/12.

77
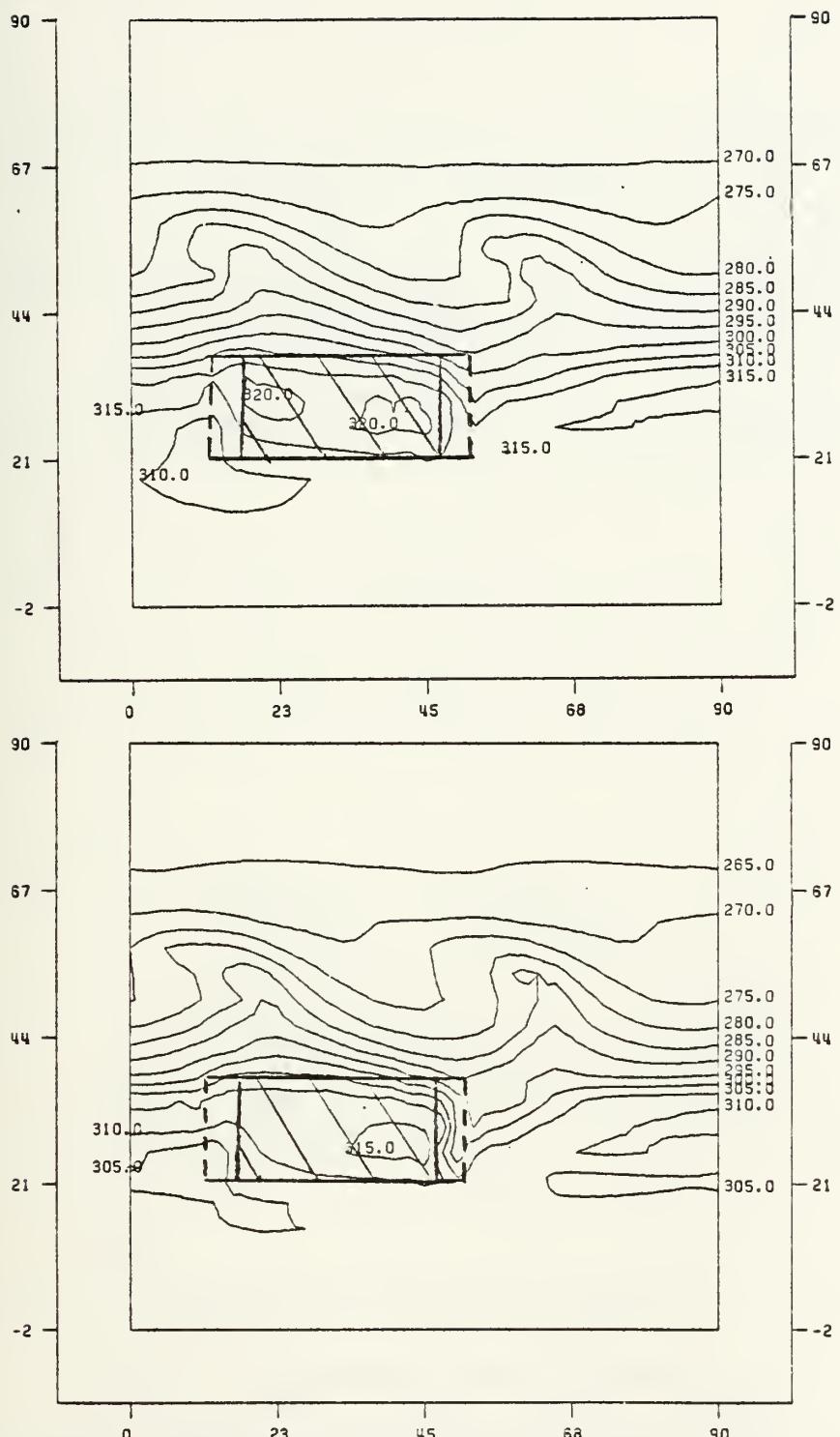
Figure 25. Potential Temperature, 96 h, Exp. 4. Sigma = 9/12, 11/12.
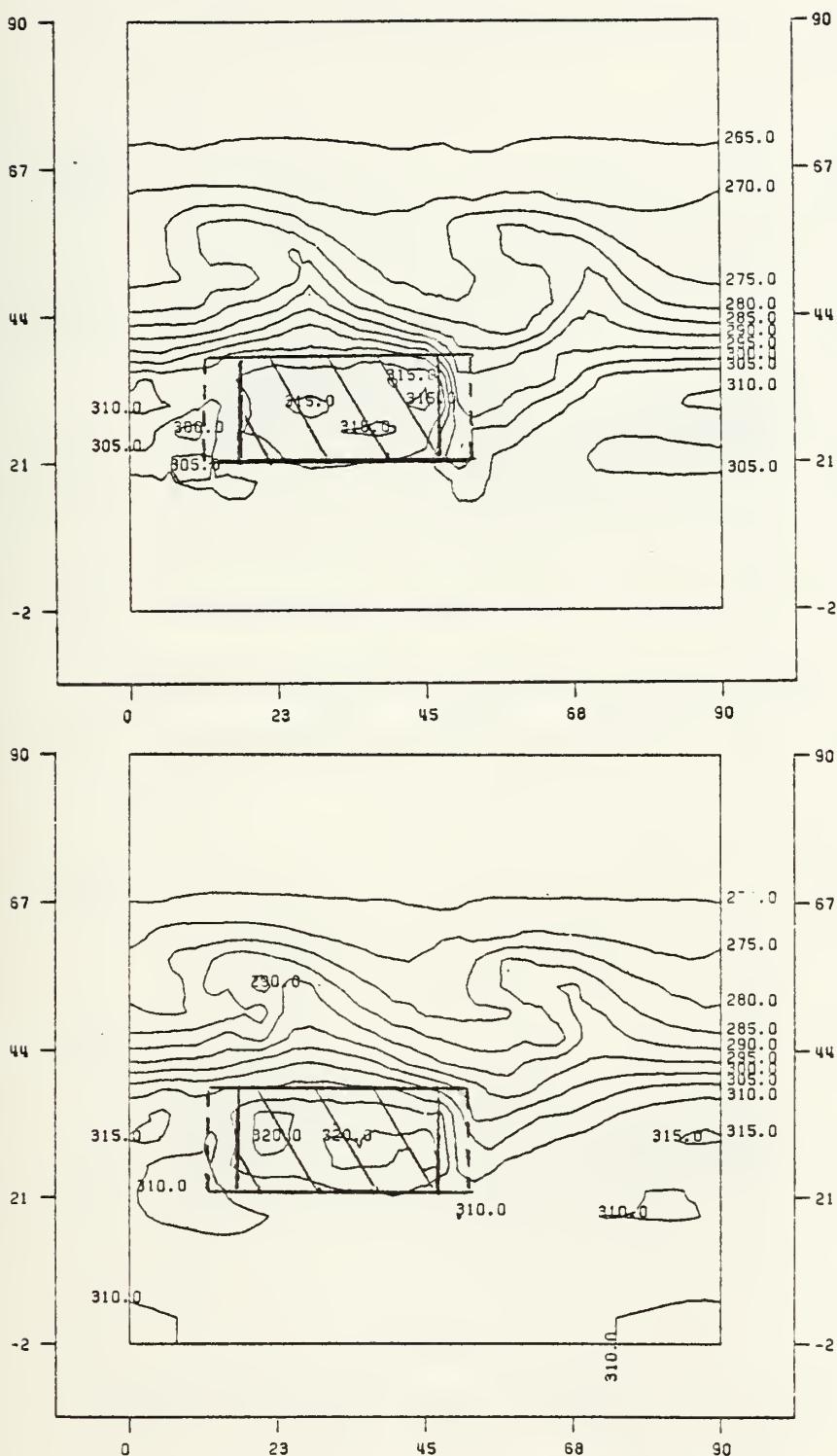
Figure 26. Potential Temperature, 108 h, Exp. 4. Sigma = 9/12, 11/12.
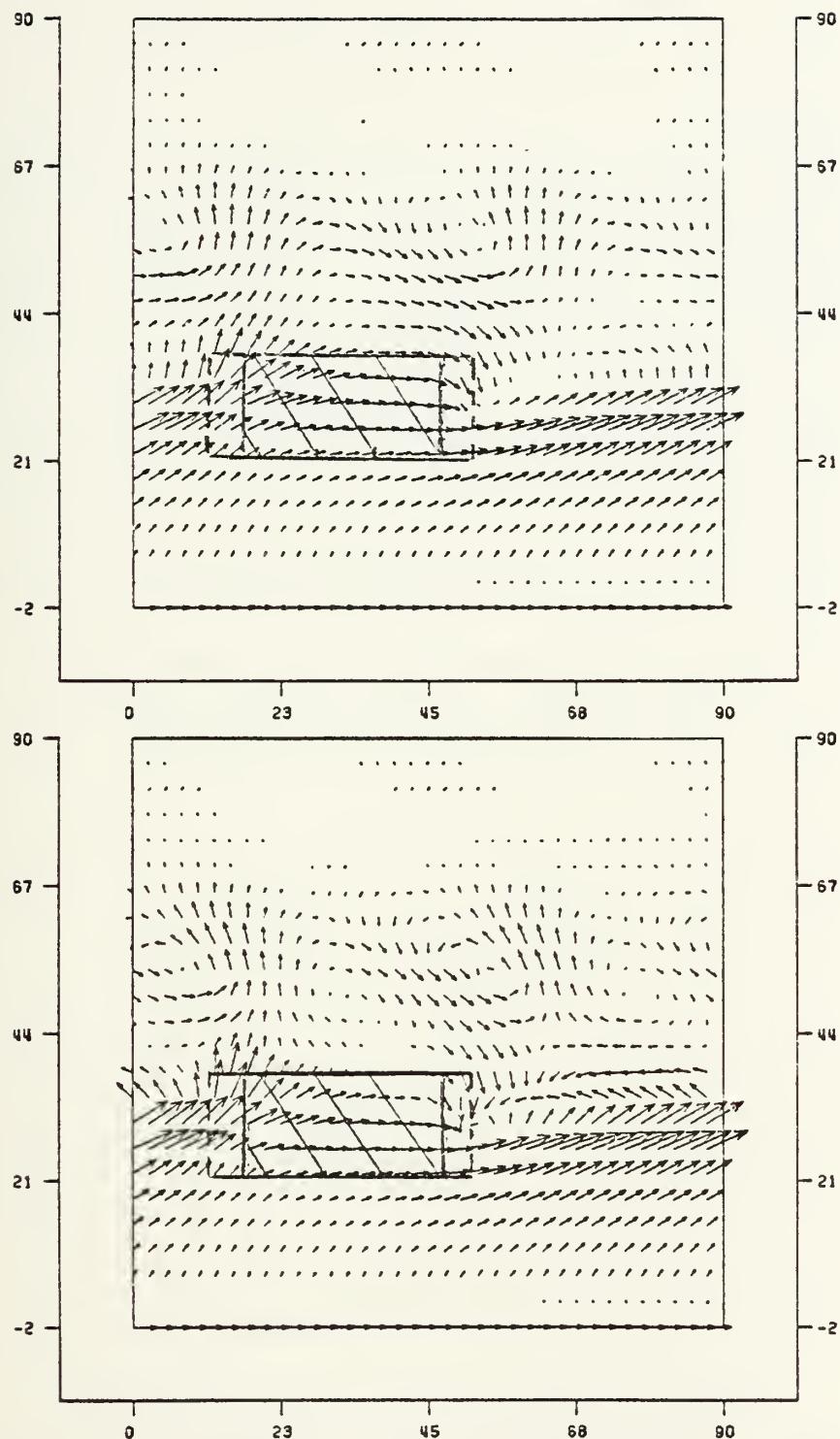
Figure 27. Wind Vectors, 84 h, Experiment 4. Sigma = 9/12, 11/12.
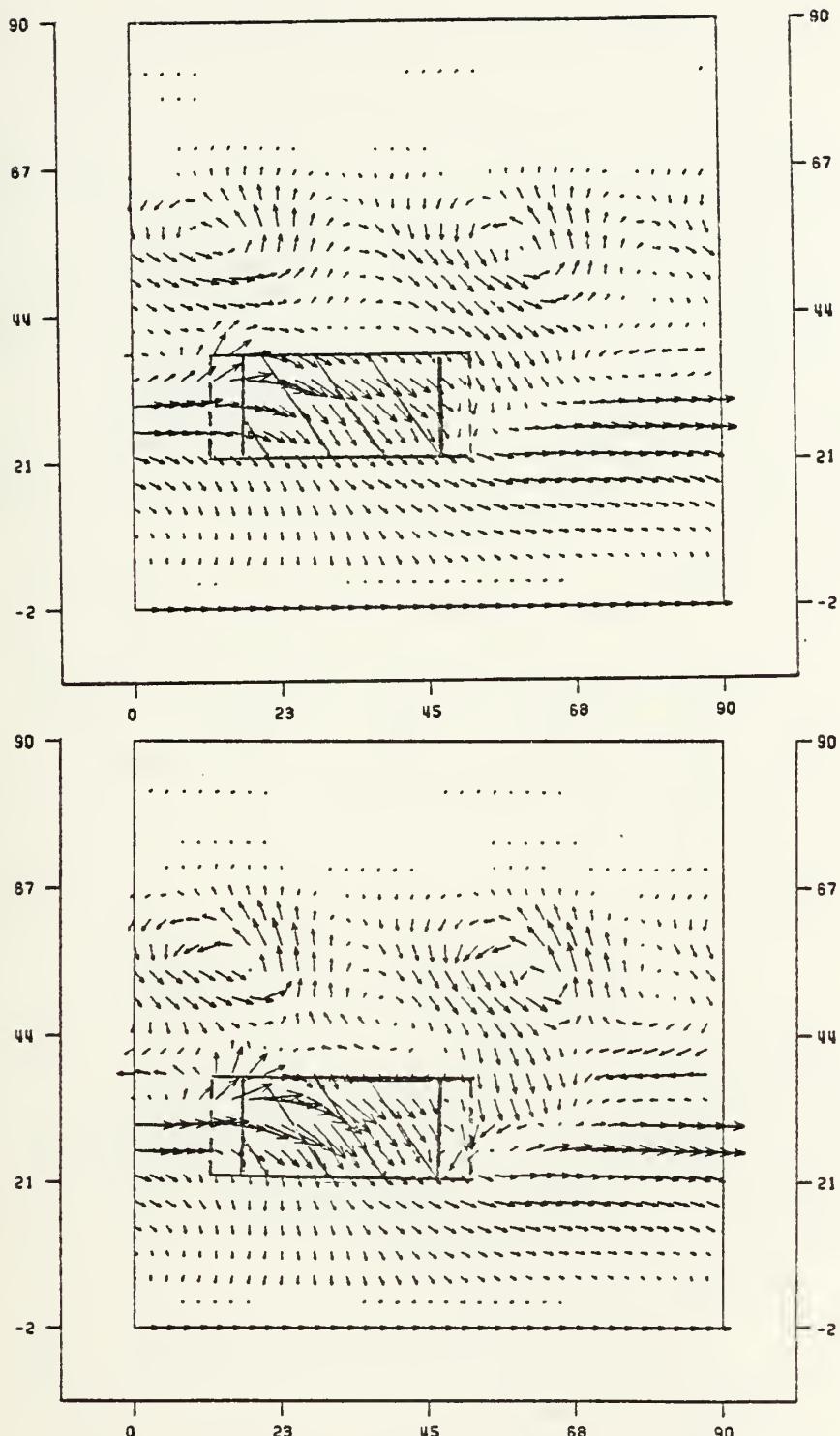
Figure 28.   Wind Vectors, 96 h, Experiment 4.   Sigma = 9/12, 11/12.
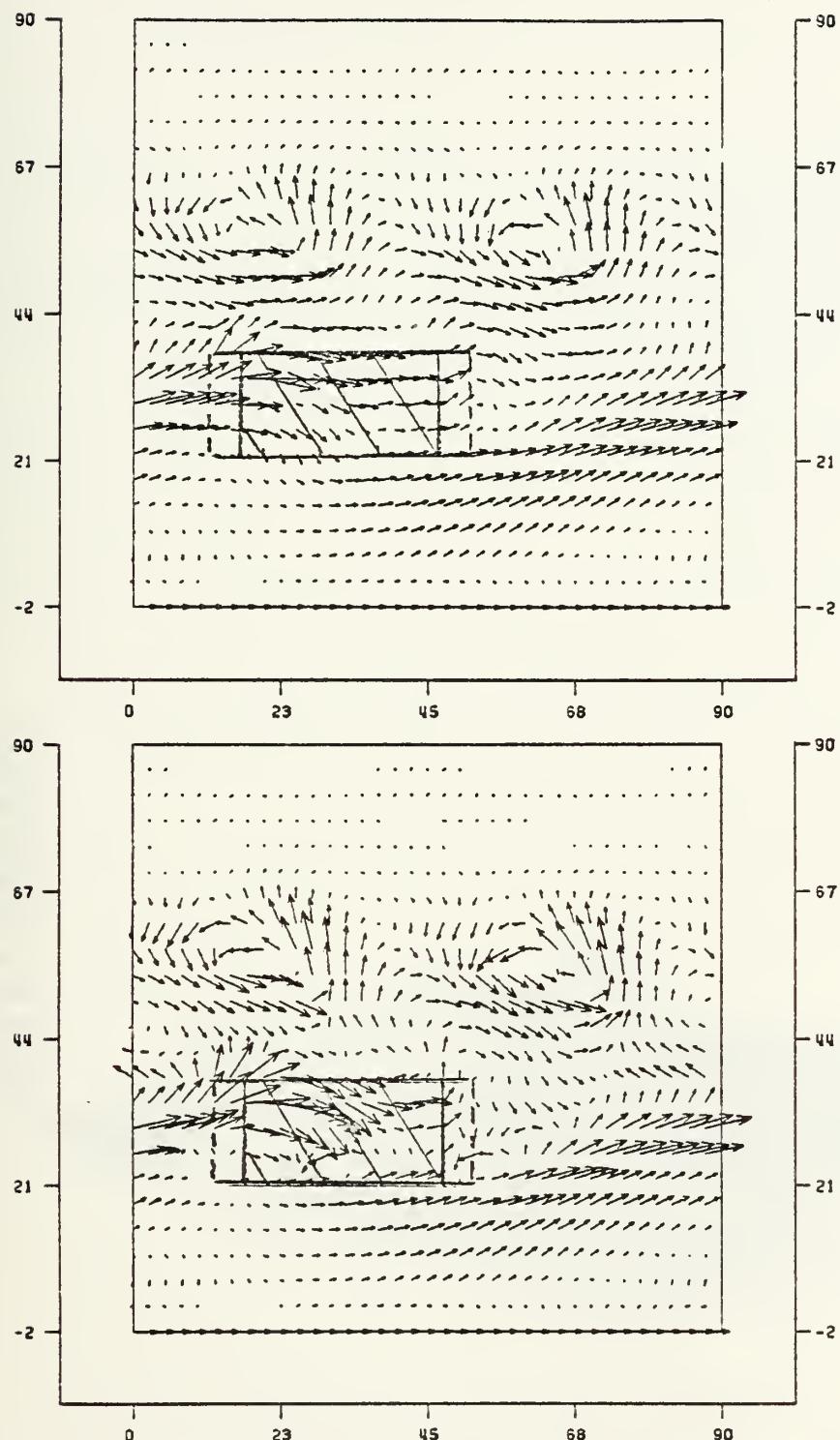
Figure 29. Wind Vectors, 108 h, Experiment 4. Sigma =
9/12, 11/12.

82
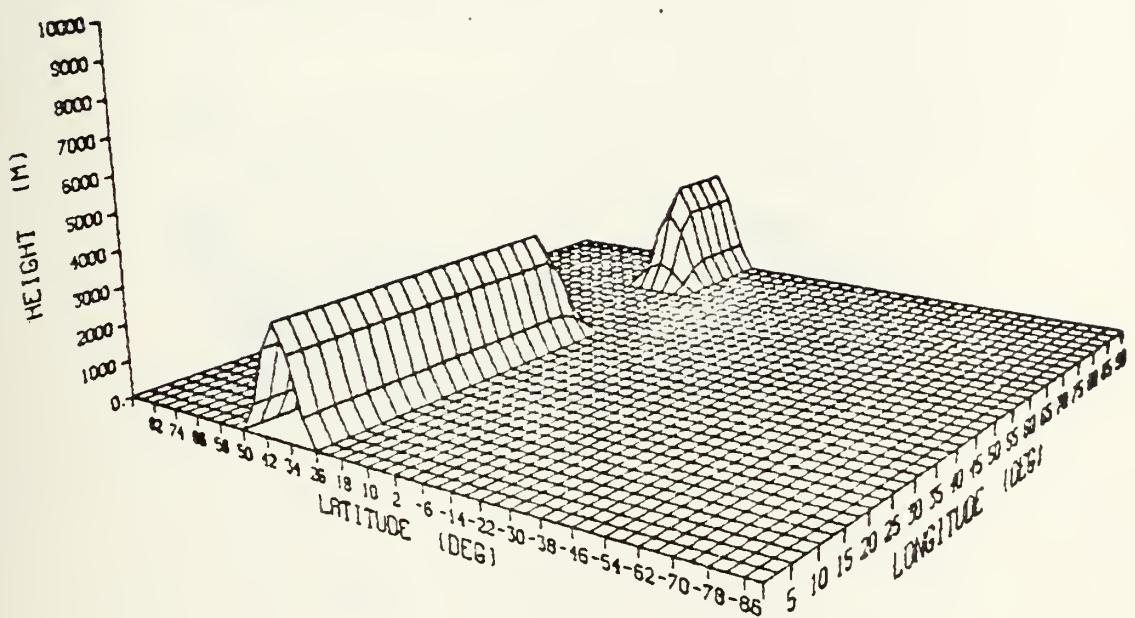
Figure 30. Model Terrain, Experiment 5.

83
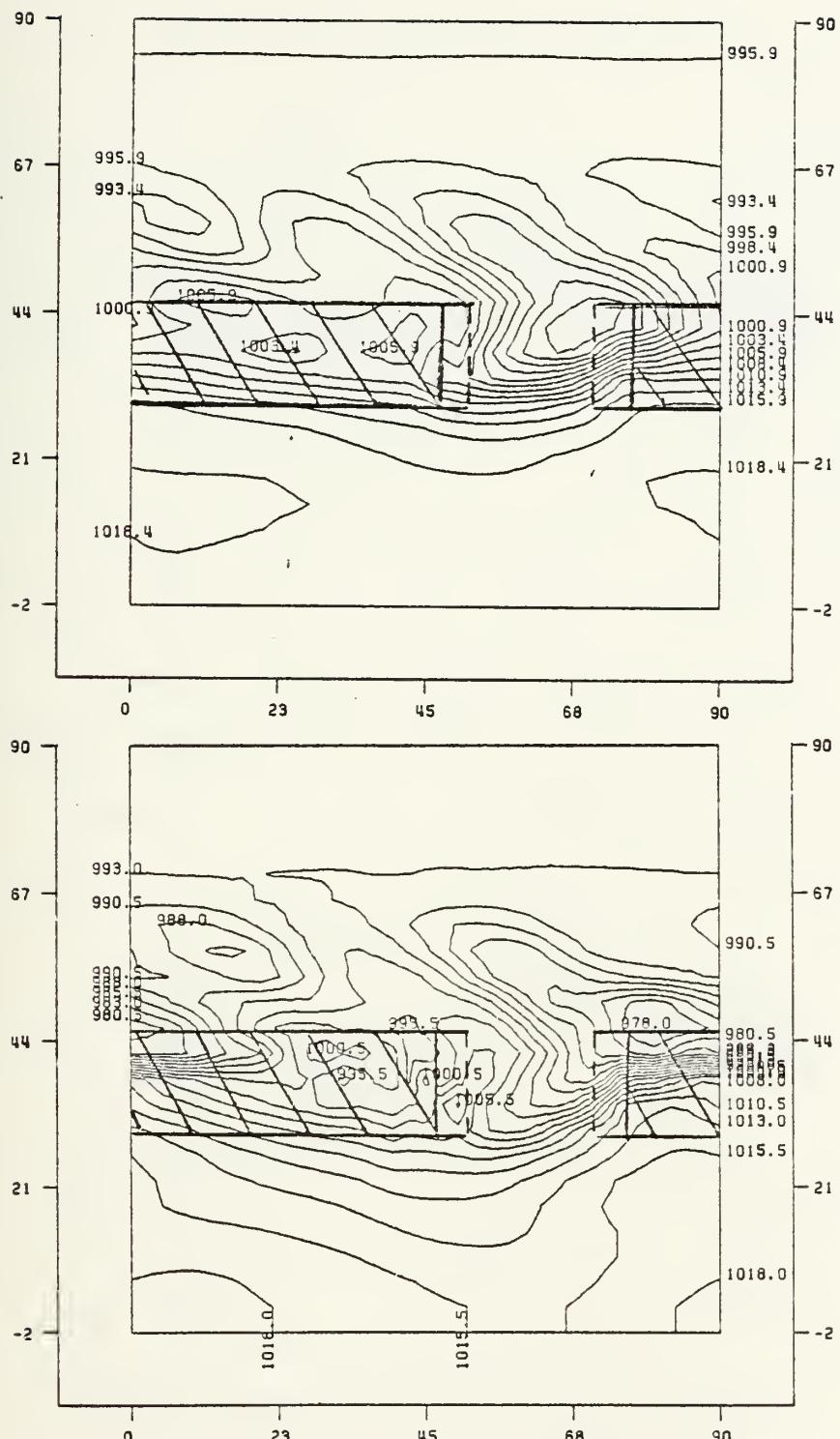
Figure 31.   Sea-Level Pressure, 90 and 102 h, Exp. 5.
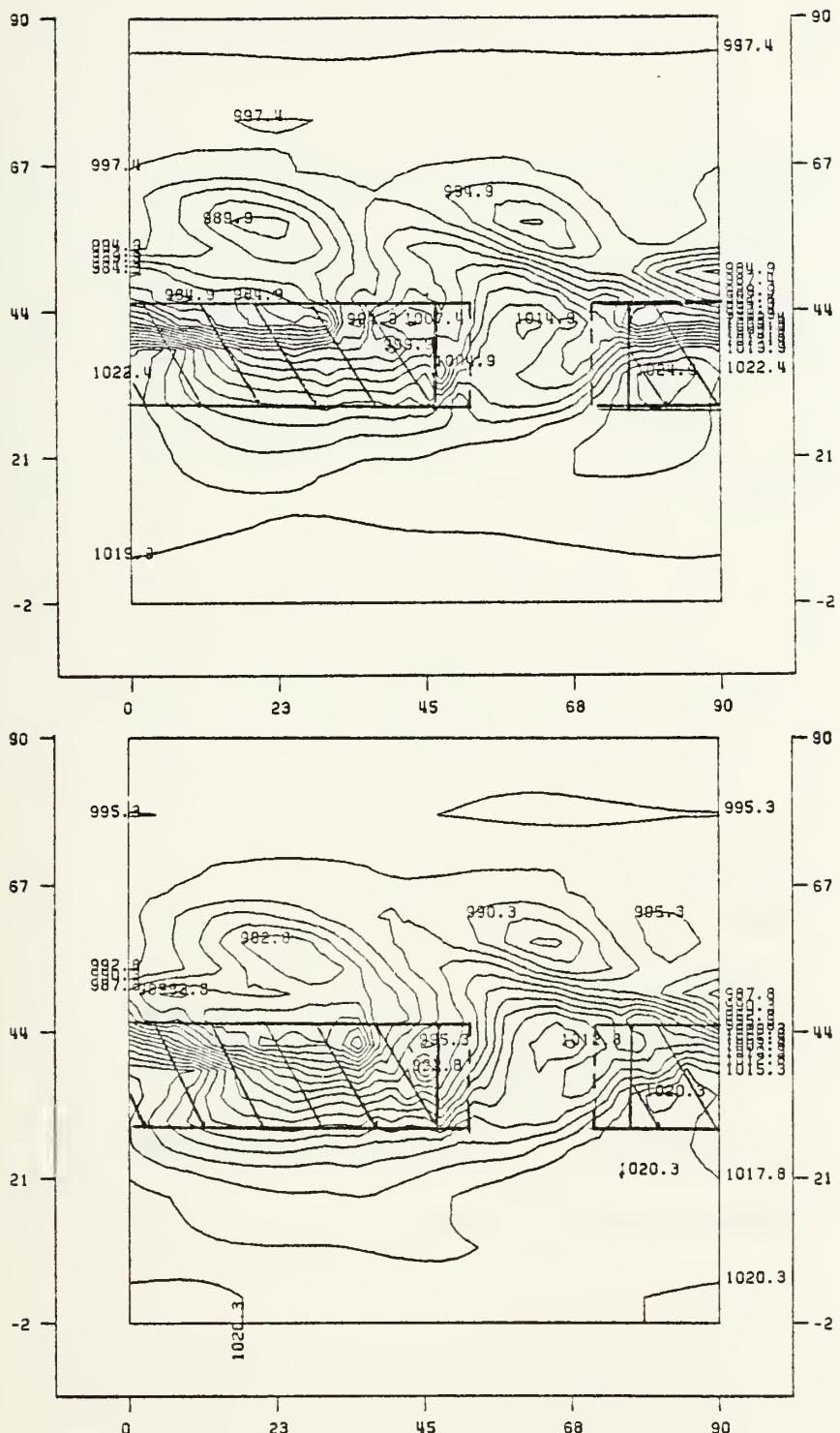
Figure 32. Sea-Level Pressure, 114 and 120 h, Exp. 5.

85
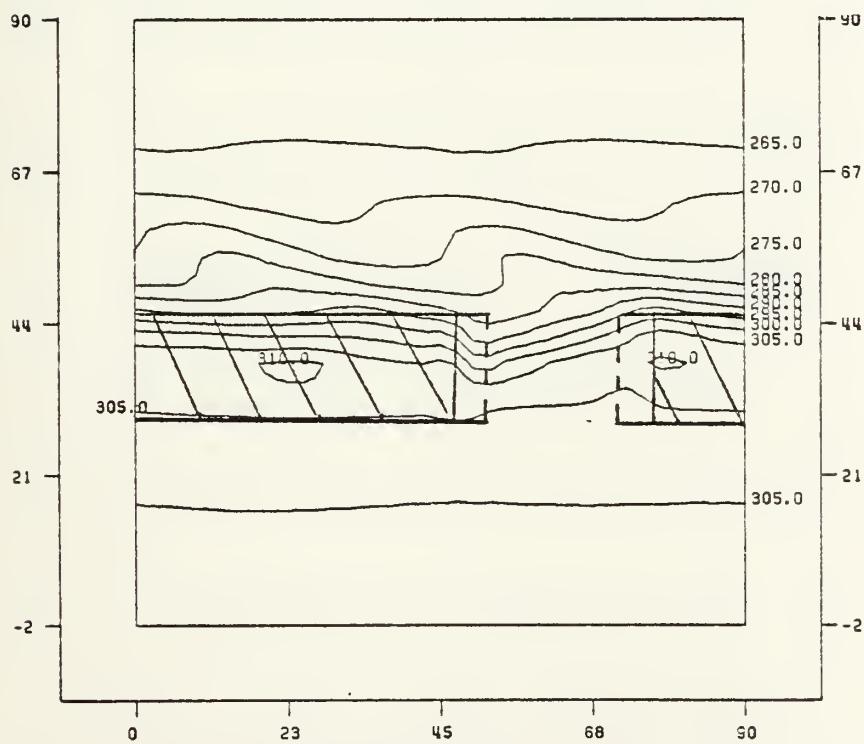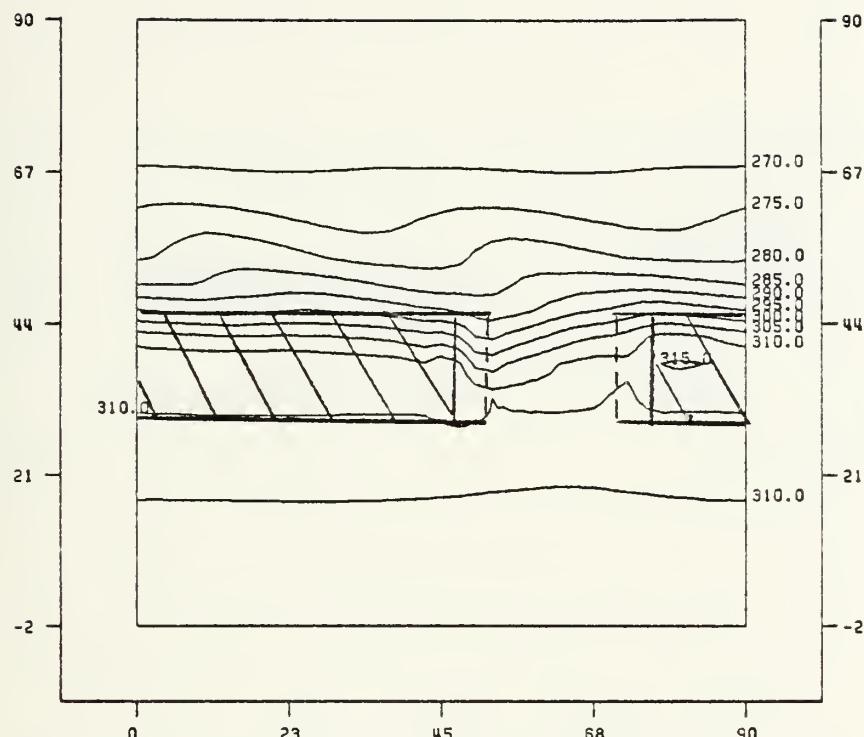
Figure 33. Potential Temperature, 90 H, Exp. 5. Sigma = 9/12, 11/12.
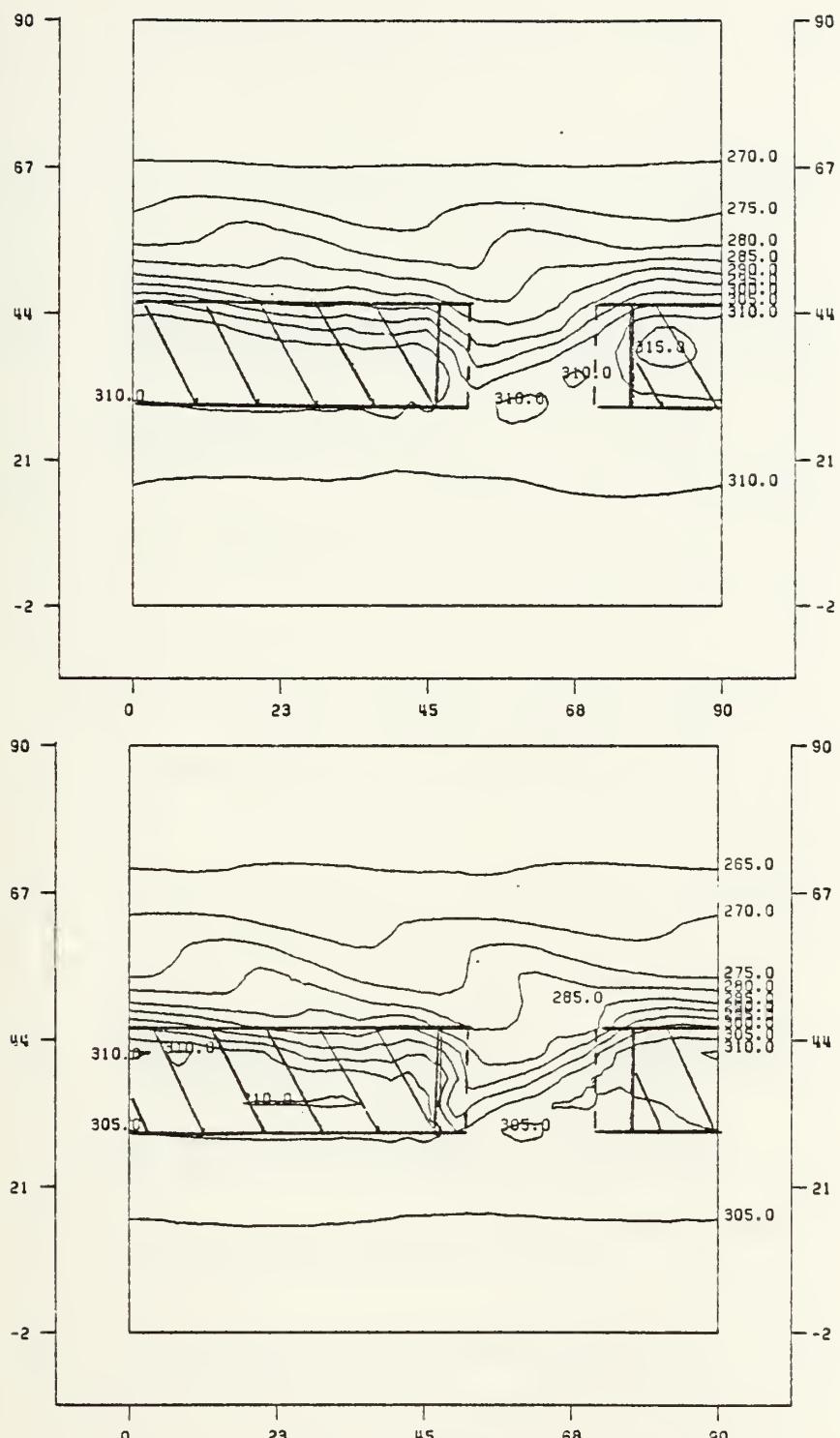
Figure 34. Potential Temperature, 102 h, Exp. 5. Sigma = 9/12, 11/12.
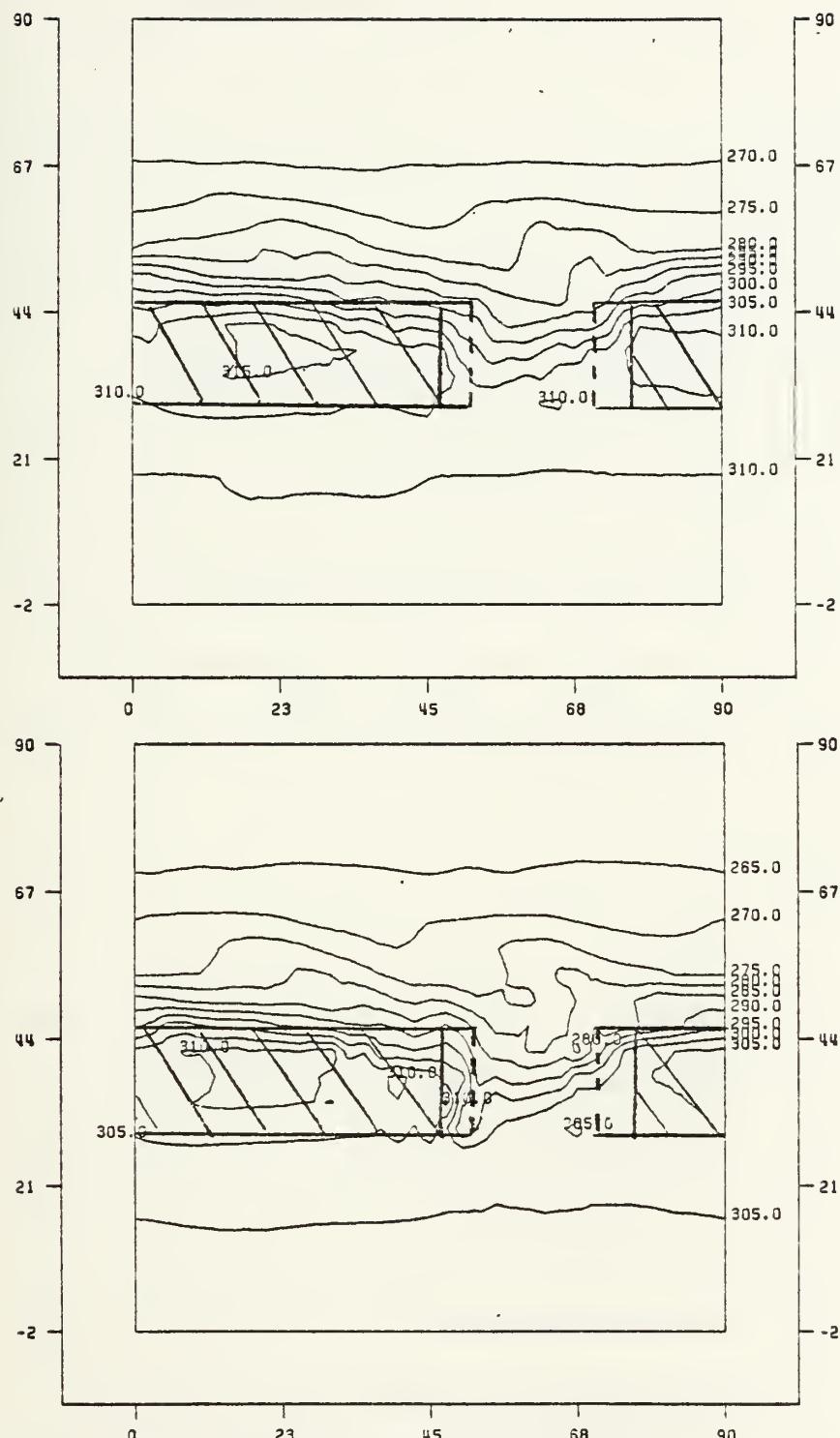
Figure 35. Potential Temperature, 114 h, Exp. 5. Sigma = 9/12, 11/12.
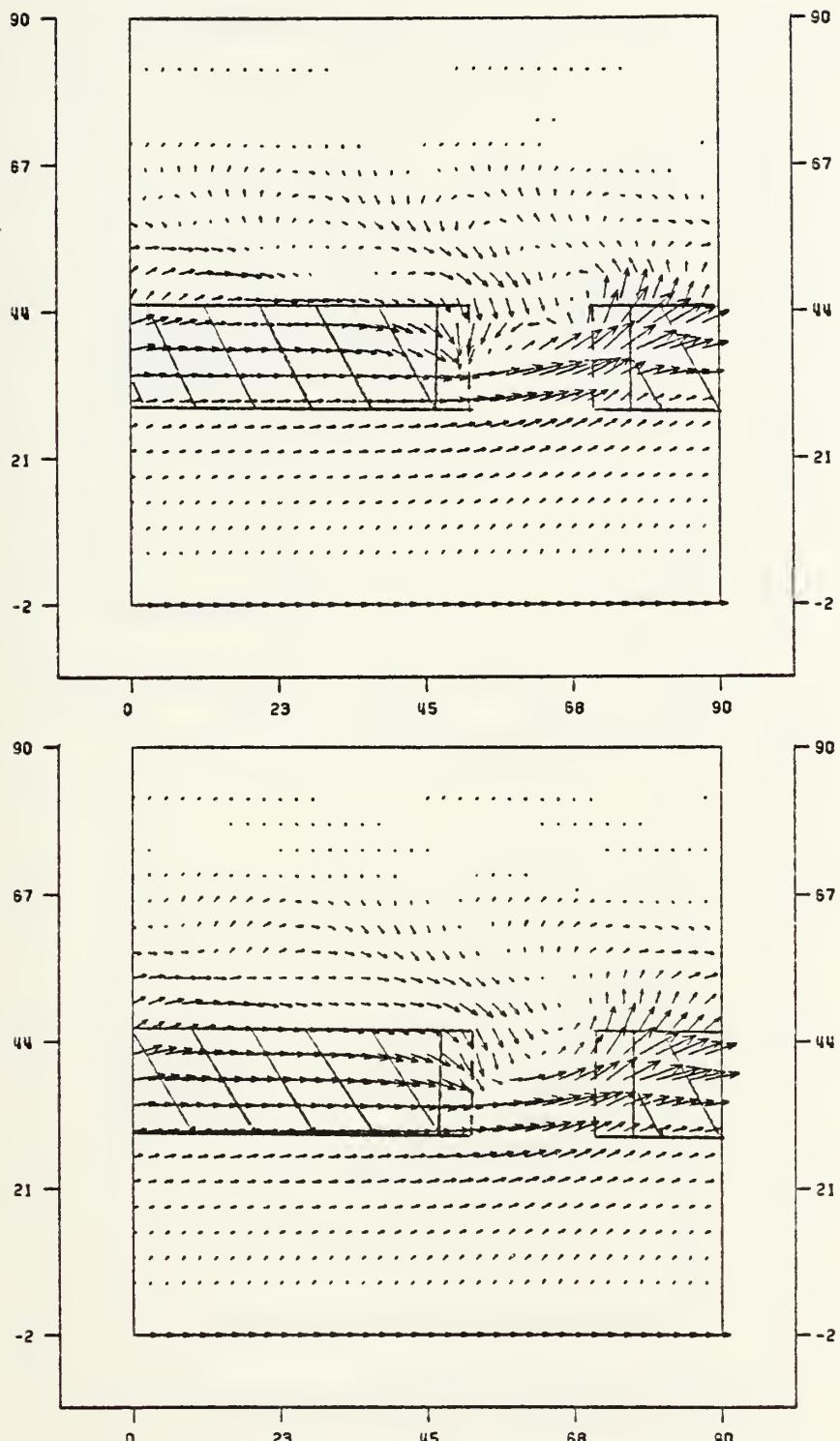
Figure 36. Wind Vectors, 90 h, Experiment 5. Sigma = 9/12, 11/12.
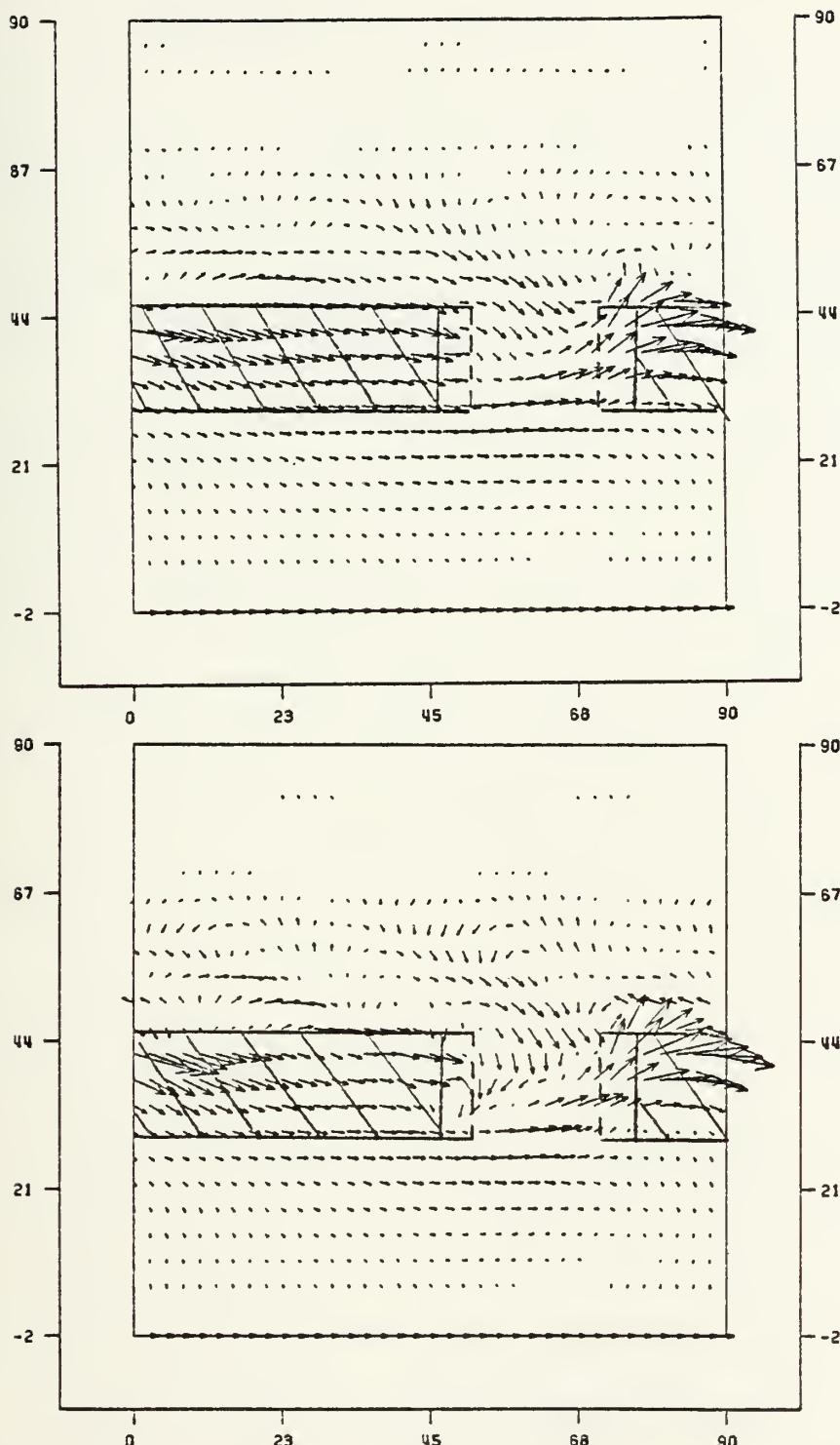
Figure 37. Wind Vectors, 102 h, Experiment 5. Sigma = 9/12, 11/12.
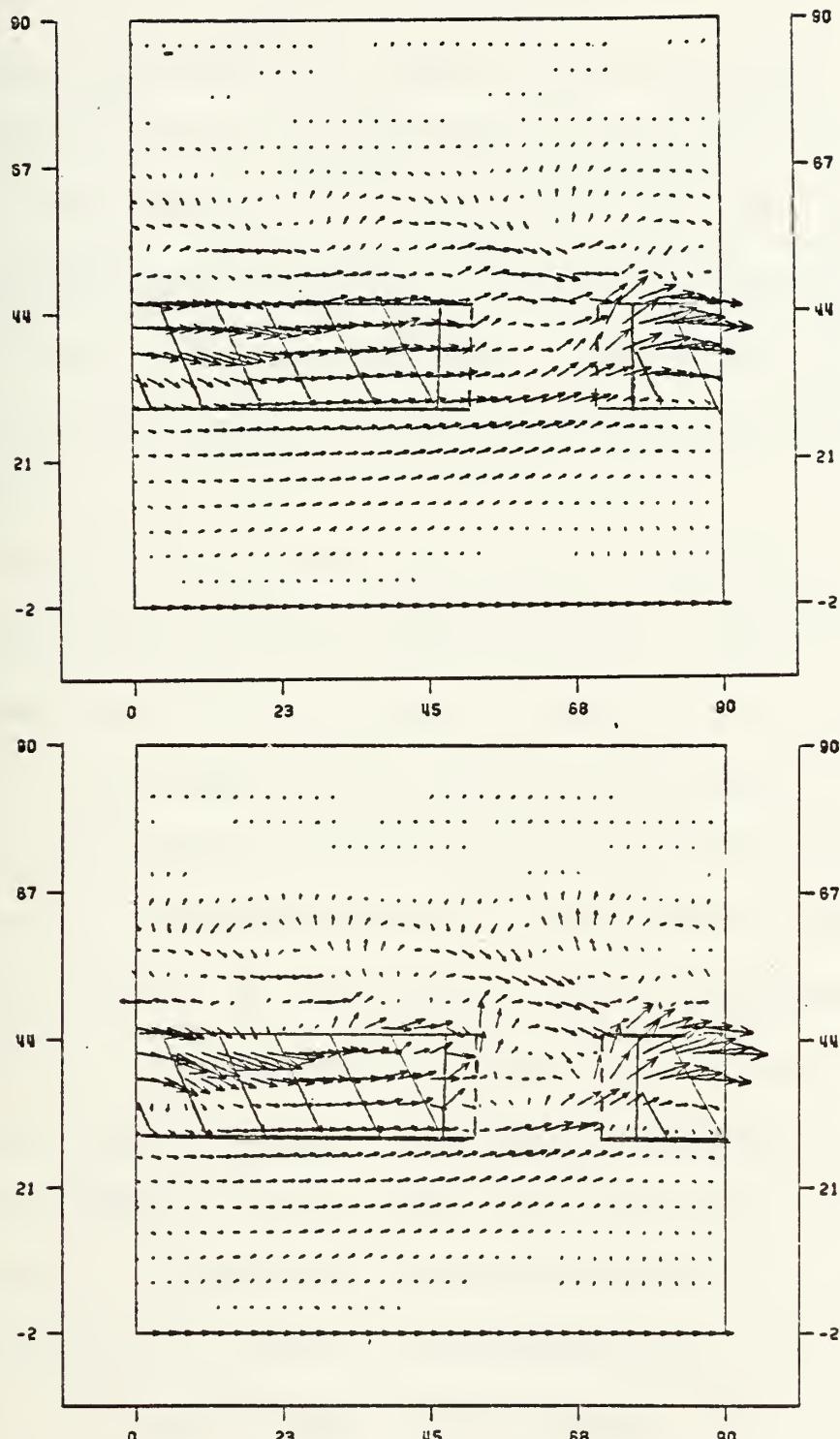
Figure 38.   Wind Vectors, 114 h, Experiment 5.   Sigma = 9/12, 11/12.

V. CONCLUSIONS

The interaction of a mid-latitude baroclinic wave with several different mountain-valley configurations was examined. The purpose was to determine the contribution made by a well-developed baroclinic wave to the initiation of monsoon surges. It was found that these waves can initiate a monsoon surge although such surges are weak and limited in extent.

The mountains in each experiment are an east-west range located south of the mid-latitude wave. As was first noted in Experiment #2 the mountains appear to have a stabilizing effect on the growth of the wave. The effect is especially evident when the mountains are placed farther north, nearer the center of the disturbance. The reduced growth rate is probably caused by the blocking of the v-component of the wind by the mountain barrier to the south. This would slow the wave growth because the energy conversion is porportional to $\overline{v'\theta'}$. Walker (1982) also found this effect with a disturbance moving along the north side of a mountain range.

Previously, several observations were made about the nature of monsoon surges. These include: (1) the occurrence of rapid, ageostrophic flow from high to low pressure, (2)

strengthening of the north-northeasterly winds, (3) a sharp drop in surface temperature and (4) the shallow structure of the surge. To some extent, each of these characteristics is simulated by one or more of the experiments.

Experiment #6, in which only the zonal mean flow interacts with the terrain, shows no evidence of a surge. All other experiments, in which the perturbation is added to the mean flow, do produce weak monsoon surges. This indicates the eastward-moving anticyclone associated with the mid-latitude baroclinic wave is the source of the surges occurring in this study.

In Experiments 3 and 4 the mountains are centered at 30°N, the western edge of each valley is located at the same point although the fourth valley is twice the size of the third. In each case a cold, high pressure airmass moves southward along the western valley wall during the twelve hours following completion of the valley. The leading edge of the surge is ageostrophic.

Figs. 39 and 40 show the change of potential temperature with time in the valley for Experiments 3 and 4. The profiles extend from 14°N to 46°N along the western valley floor (55° long), the valley is located between 22°N and

38°N. In each case little, if any, change in temperature occurs at 14°N although at 18°N the temperature decreases 7K between 96 and 108 h. In the valley the maximum temperature change occurs earlier, between 84 and 96 h, and is much larger, -16K and -17K at 26°N. The surge is well defined within the valley but dissipates rapidly south of 22°N. This is indicative of the weak character of the monsoon surges in this study since the cold air in observed cases has been traced well into the tropical regions while in these experiments it cannot be found even eight degrees south of the valley.

As can be seen the results of the two experiments are nearly identical, indicating the size of the valley is not an important consideration.

The oscillation in the pressure (mass) field is apparently a gravity wave, the result of an inward rush of air filling the "vacuum" produced by the creation of the valley. It has roughly a 24-h period, which may be related to the twelve hour period in which the valley is built, and it slowly dampens during the subsequent 60 h of the experiment. It has no observable effect on the pressure gradients and was not evident in either the potential temperature or the wind fields. The oscillation also occurs in Experiment #5.

In Experiment #5 the rapid southward movement of the cold airmass occurs only during the first six hours after valley completion. This is due to the placement of the mountains at 38°N resulting in a much weaker disturbance. Fig. 41 shows the change in potential temperature with time in the valley. The valley is located between 30°N and 46°N, the profile is along the western valley floor.

The decrease in temperature is evident in the valley between 90 and 102 h. As in Experiments 3 and 4 the cold air can be traced only four degrees south of the valley. Unlike the two previous experiments warming occurs during the second twelve hour period, due to the re-development of the anticyclone within the valley. The southerly winds in the western region of the anticyclone prevent the flow of cold air into the valley and effectively "shut off" the surge.

The monsoon surges initiated in these experiments are evident only in the lowest sigma levels, at sigma = 11/12, 9/12 and 7/12. In a standard atmosphere, over flat terrain, these correspond to pressure heights less than 675 mb. The surge is strongest at the lowest level and dissipates with height, becoming very weak at sigma = 7/12. This is

observed in both the wind and potential temperature fields in all experiments and agrees closely with the definition of the monsoon surge as a low-level, or surface, phenomenon.

These results suggest that the mid-latitude baroclinic wave can initiate monsoon surges. The surges are weak and limited to the valley but otherwise exhibit the characteristics of observed monsoon surges. The weakness of these surges indicates other forcing mechanisms are necessary in order to adequately model the monsoon surge. These may include a strong, stationary high located northwest of the valley similar to the anticyclone associated with the winter monsoon. Other analytical studies indicate that an upper-tropospheric, planetary scale wave number three is necessary for the occurrence of strong monsoon surges. Such a wave positioned with the ridge to the west of the surface anticyclone would result in strong northwesterly flow over the high pressure center. This would initiate cold air advection throughout the troposphere and increase subsidence over the surface anticyclone leading to stronger surges. Weak monsoon surges were associated with near zonal flow at higher altitudes, this describes the upper-level flow used in these experiments. The inclusion of one or both of these

96

phenomena may result in stronger, more extensive monsoon surges than those observed in this study.
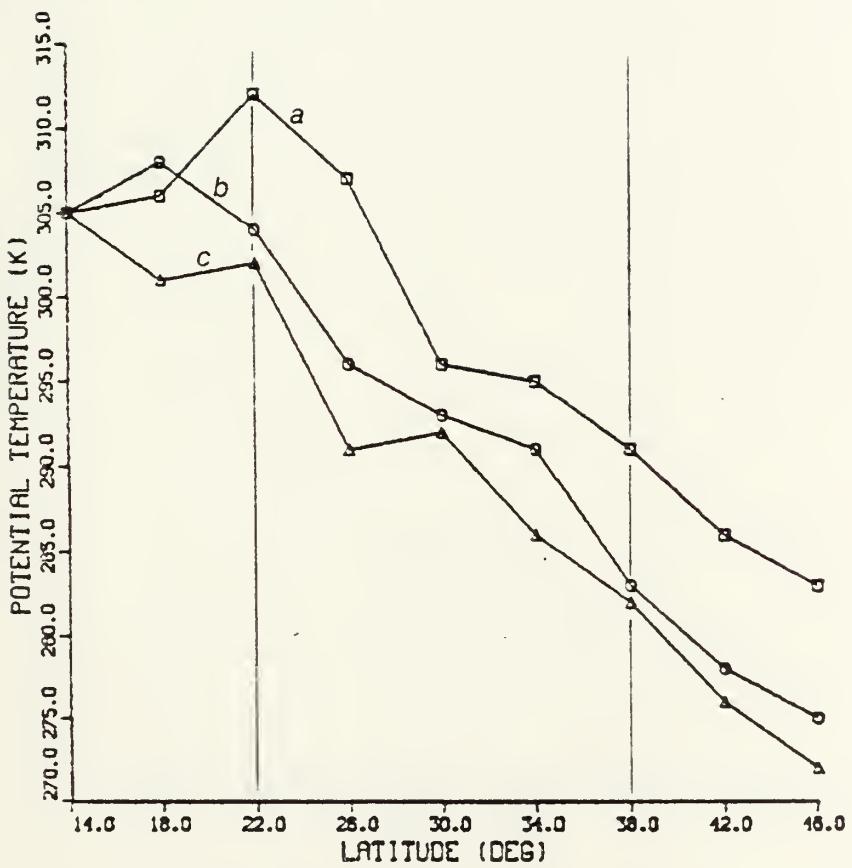
Figure 39. Potential Temperature vs Latitude, Exp. 3.
Vertical lines represent valley boundaries. (a)
84 h, (b) 96 h and (c) 108 h.
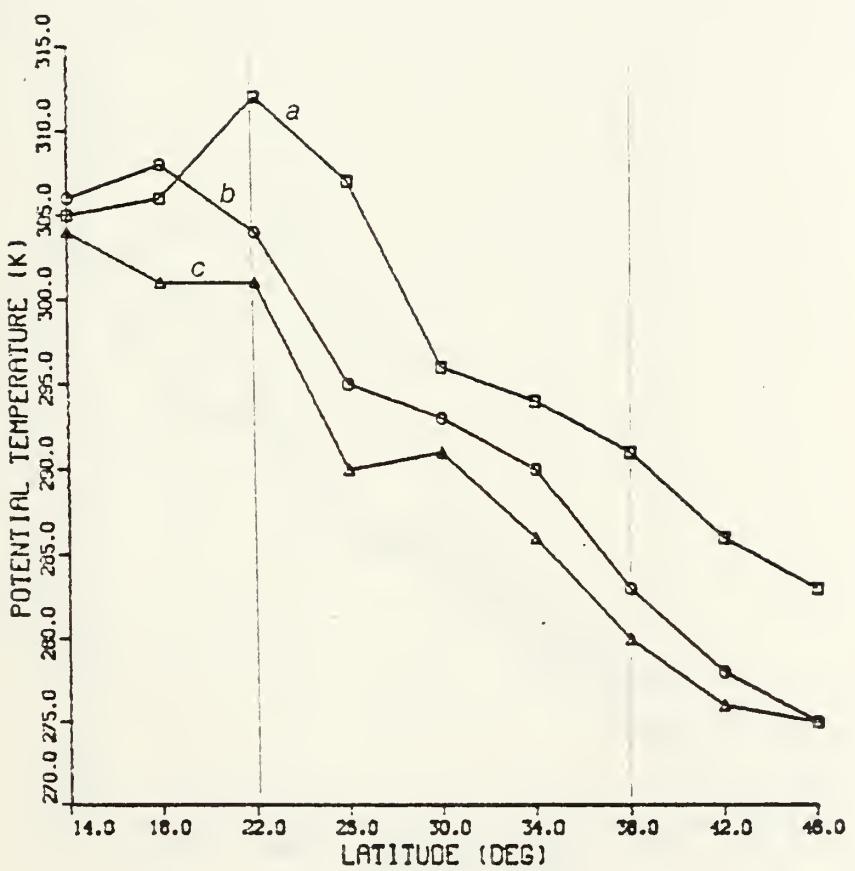
Figure 40. Potential Temperature vs Latitude, Exp. 4. Vertical lines represent valley boundaries. (a) 84 h, (b) 96 h and (c) 108 h.
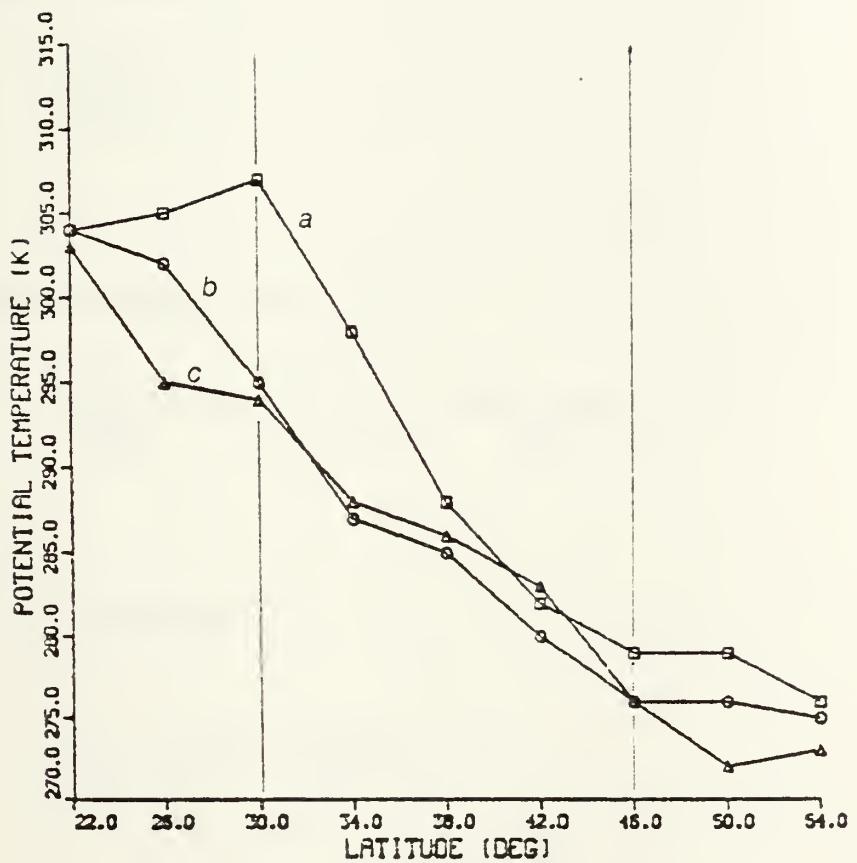
Figure 41. Potential Temperature vs Latitude, Exp. 5.
Vertical lines represent valley boundaries. (a)
90 h, (b) 102 h and (c) 14 h.

APPENDIX A

MODEL PRIMITIVE EQUATIONS

Equation of State:

$$p\alpha = RT$$

Hydrostatic Equation:

$$\frac{\partial \phi}{\partial \sigma} = -\pi\alpha$$

Horizontal Momentum Equations:

$$\Pi\left(\frac{d\tilde{v}}{dt}\right) + f\hat{k}\ \Pi\tilde{v} + \tilde{\nabla}_{\sigma}(\Pi\phi) - \tilde{\nabla}\Pi\ \frac{\delta}{\delta\sigma}(\phi\sigma) = 0$$

Continuity Equation:

$$\frac{\delta\Pi}{\delta t} + \tilde{\nabla}_{\sigma}\cdot(\Pi\tilde{v}) + \frac{\delta}{\delta\sigma}(\Pi\dot{\sigma}) = 0$$

1st Law of Thermodynamics:

$$\frac{\delta}{\delta}(\Pi Cp\ln\theta) + \tilde{\nabla}\cdot(\Pi\tilde{V}Cp\ln\theta) + \frac{\delta}{\delta\sigma}(\Pi\dot{\sigma}Cp\ln\theta) = 0$$

102

APPENDIX B

LIST OF SYMBOLS

a	radius of the earth
A	amplitude of the perturbation
Cp	specific heat at constant pressure
f	coriolis parameter
fo	value of coriolis parameter at 45N
F	force
g	gravitational acceleration
n	wave number
P	pressure (P = P + P')
Po	surface pressure at 45N, 1013.25 mb
Pm	maximum model pressure height, 125 mb
R	gas constant for air
T	temperature
To	surface temperature at 45N, 288K
U	zonal velocity component (U = U + U')
Um	maximum velocity, surface: 5 m/s, upper: 65 m/s
V	meridional velocity component (V = V + V')
Z	terrain height
α	specific volume
γ	halfwidth of jet
Γ	dry adiabatic lapse rate, 6.5 K/km
Θ	potential temperature
λ	longitude
π	3.14159
Π	normalized pressure
σ	vertical coordinate
$\dot{\sigma}$	vertical velocity in sigma coordinate system
τ	model time
τ_i	model time at which terrain growth begins
τ_f	model time at which terrain reaches final height
φ	latitude

Φ_o latitude of jet

Φ_1 latitude at which mountain range is centered

Φ geopotential, also current terrain height

Φ_f maximum terrain height, 3000 m

Ω angular velocity of the earth

Arakawa, A., and V. Lamb, 1977: Computational Design of the
Basic Dynamical Processes of the UCLA General Circulation
Model. Methods in Computational Physics, Vol.17, Academic
Press, 337 pp.

Arakawa, A., and V. Lamb, 1981: A Potential Enstrophy and
Energy Conserving Scheme for the Shallow Water Equations.
Mon. Wea. Rev., 109, 18-36.

Chang, C.-P., G.T.J. Chen, and J.E. Millard, 1983:
Gravitational Character of Cold Surges during Winter MONEX.
Mon. Wea. Rev., 111, 293-307.

Chang, C.-P., J.E. Erickson, and K.M.W. Lau, 1979:
Northeasterly Cold Surges and Near-Equatorial Disturbances
over the Winter MONEX Area during December 1974. Part I:
Synoptic Aspects. Mon. Wea. Rev., 107, 812-829

Chang, C.-P., and K.M.W. Lau, 1980: Northeasterly Cold
Surges and Near-Equatorial Disturbances over the Winter
MONEX Area during December 1974. Part II: Planetary-Scale
Aspects. Mon. Wea. Rev., 108, 298-312.

Chang, C.-P., K.M.W. Lau, 1982: Short-Term Planetary-Scale
Interactions over the Tropics and Midlatitudes during
Northern Winter. Part I: Contrasts between Active and
Inactive Periods. Mon. Wea. Rev., 110, 933-946.

Chu, E.W.K., 1978: A Method for Forecasting the Arrival of
Cold Surges in Hong Kong. Royal Observatory Technical Note
No. 43, 31 pp.

Danielsen E.F., and F.P. Ho, 1969: An isentropic Trajectory
Study of a Strong Northeast Monsoon Surge. Air Force
Cambridge Research Laboratories, Report No. 69-0036, 13 pp.

Haltiner G.J., and R.T. Williams, 1980: Numerical Weather
Prediction and Dynamic Meteorology. John Wiley and Sons,
477 pp.

Lim, H., and C.-P. Chang, 1981: A Theory for Midlatitude
Forcing of Tropical Motions during Winter Monsoons. J.
Atmos. Sci., 38, 2377-2392.

Murakami, T., 1979: Winter Monsoon Surges over East and
Southeast Asia. J. Meteor. Soc. Japan, 57, 133-158.

Ramage, C.S., 1971: Monsoon Meteorology. Academic Press,
296 pp.

Walker, J., 1982: Numerical Simulation of the Influence of Small Scale Mountains Ranges on a Baroclinic Wave. M.S. Thesis, Naval Postgraduate School, 159 pp.

INITIAL DISTRIBUTION LIST

No. Copies

1. Chairman (Code 63Rd)
   Department of Meteorology
   Naval Postgraduate School
   Monterey, CA 93943

   1

2. Professor Roger T. Williams, Code 63Wu
   Department of Meteorology
   Naval Postgraduate School
   Monterey, CA 93943

   8

3. Professor C.-P. Chang, Code 63Cp
   Department of Meteorology
   Naval Postgraduate School
   Monterey, CA 93943

   1

4. Chairman (Code 68Mr)
   Department of Oceanography
   Naval Postgraduate School
   Monterey, CA 93943

   1

5. Capt. Beverley J. Baker
   Detachment 1, 2WS
   Wright-Patterson AFB, OH 45433

   3

6. Capt. Alan R. Shaffer, Code 63
   Department of Meteorology
   Naval Postgraduate School
   Monterey, CA 93943

   1

7. Library, Code 0142
   Naval Postgraduate School
   Monterey, CA 93943

   2

8. Commander
   Air Weather Service
   Scott AFB, IL 62225

   1

9. Commanding Officer
   Air Force Global Weather Central
   Offutt AFB, NE 68113

   1

10. Program Manager, AFIT/CIRF
    Air Force Institute of Technology
    Wright-Patterson AFB, OH 45433

    1

11. Commanding Officer
    Fleet Numerical Oceanography Center
    Monterey, CA 93940

    1

12.   Commanding Officer   1
        Naval Environmental Prediction Research Facility
        Monterey, CA 93940

13.   Defense Technical Information Center   2
        Cameron Station
        Alexandria, VA 22314

14.   Commander   1
        Naval Oceanography Command
        NSTL Station
        Bay St. Louis, MS 39522

15.   Commanding Officer   1
        Naval Oceanographic Office
        NSTL Station
        Bay St. Louis, MS 39522

16.   Office of Naval Research (Code 420)   1
        Naval Ocean Research and Development Activity
        800 N. Quincy Street
        Arlington, VA 22217

17.   Chairman, Oceanography Department   1
        U.S. Naval Academy
        Annapolis, MD 21402

18.   Chief of Naval Research   1
        800 N. Quincy Street
        Arlington, VA 22217

19.   Director Naval Oceanography Division   1
        Naval Observatory
        34th and Massuchusetts Ave. NW
        Washington, DC 20390

20.   Commanding Officer   1
        Naval Ocean Research and Development Acitivity
        NSTL Station
        Bay St. Louis, MS 39522

21.   Dr. A. Arakawa   1
        Department of Meteorclogy
        University of California
        Los Angeles, CA 90024

22.   Dr. R.L. Elsberry, Code 63Es   1
        Department of Meteorology
        Naval Postgraduate School
        Monterey, CA 93943

23.   Dr. J. Young   1
        Department of Meteorology
        University of Wisconsin
        Madison, Wisconsin 53706

24.　Dr. A. Kasahara　　　　　　　　　　　　　　　　1
　　　National Center for Atmospheric Research
　　　P.O. Box 3000
　　　Boulder, Colorado　80303

25.　Dr. E.C. Nickerson　　　　　　　　　　　　　　1
　　　NOAA, Atmospheric Physics & Chemistry Laboratory
　　　Boulder, Colorado　80302

26.　Prof. N.A. Phillips　　　　　　　　　　　　　1
　　　National Meteorological Center/NOAA
　　　World Weather Building
　　　Washington, D.C.　20233

27.　Dr. J. Smagorinsky, Director　　　　　　　　1
　　　Geophysical Fluid Dynamics Laboratory
　　　Princeton University
　　　Princeton, New Jersey　08540

28.　Dr. T. Rosmond　　　　　　　　　　　　　　　　1
　　　Naval Environmental Prediction Research Facility
　　　Monterey, CA　93940

29.　Dr. Y. Sasaki　　　　　　　　　　　　　　　　1
　　　Department of Meteorology
　　　University of Oklahoma
　　　Norman, Oklahoma　73069

30.　Dr. C.H. Wash, Code 63　　　　　　　　　　　1
　　　Department of Meteorology
　　　Naval Postgraduate School
　　　Monterey, CA　93943

31.　Dr. Andrew Staniforth　　　　　　　　　　　1
　　　Recherce en Prevision Numerique
　　　West Isle Office Tower, 5ieme etage
　　　2121 Route Trans-Canada
　　　Dorval, Quebec H9P1J3　　Canada

32.　Dr. A. Weinstein　　　　　　　　　　　　　　1
　　　Naval Enviromental Prediction Research Facility
　　　Monterey, CA　93940

33.　Dr. R.T. Peirrehumbert　　　　　　　　　　　1
　　　Geophysical Fluid Dynamics Lab/NOAA
　　　P.O. Box 308
　　　Princeton, New Jersey　08540

34.　D.W. Blumen　　　　　　　　　　　　　　　　　1
　　　Campus Box 391
　　　University of Colorado
　　　Boulder, Colorado　80309